Politecnico di Torino

Politecnico di Torino

Master's Degree in Electrical Engineering

A.Y. 2024/2025

Graduation Session July 2025

Evaluation of Magnetic and Electric Fiedls in High Voltage Substations

Development of a model for Safety Assessment and regulatory compliance

Supervisor: Prof. Aldo Canova

Candidate: Giuseppe Pito'

Abstract

The objective of the thesis is to analyze the electromagnetic pollution generated by High Voltage electrical substations - specifically EHV/HV (Extra High Voltage/High Voltage) substations - with a focus on current regulations regarding the protection of people from exposure to electromagnetic fields. The research activity was centered on the development of a numerical code in MATLAB capable of accurately and effectively modeling the main components of substations. The resulting tool allows, starting from a limited number of input parameters, the complete description of the source geometry. It proves useful both in the preliminary design phase and for the analysis of existing installations.

The implemented code is based on classical electromagnetic formulations and adopts an integral approach that avoids discretizing the surrounding environment - such as air and ground - significantly reducing computational load. The results obtained with the code enable the identification of potential critical zones to improve the safety of electrical installations near areas accessible to the public or workers.

In addition to the full model, the thesis also examines a simplified approach for quickly estimating minimum safety distances. The results are critically analyzed to identify the limitations and potential of these models and assess their use as a practical and regulation-compliant alternative.

Finally, a theoretical case study of a 380 kV / 150 kV electrical substation is presented. The simulation of such a station allows for the observation of the resulting electric and magnetic fields and the comparison of the proposed models, providing valuable support for substation design focused on electromagnetic safety.

Ad maiorem Dei gloriam,
first cause and ultimate end
of my academic journey

"So, whether you eat or drink,
or whatever you do,
do all to the glory of God."
— Saint Paul

Table of Contents

List of Tables

List of Figures

List of MATLAB codes

Chapter 1

Introduction

In recent decades, society has undergone a profound transformation in the way energy is produced, distributed, and used. The modern world is increasingly dependent on electricity: technological evolution, the spread of electric mobility, the digitalization of infrastructure and the development of renewable energy have led to a significant increase in electromagnetic sources across the territory.

In this context, electrical substations represent essential nodes in the power transmission network. However, they also constitute significant sources of low-frequency (50/60 Hz) electric and magnetic fields, making it crucial to assess their exposure impact to ensure public health protection.

Alongside society's increasing electrification, attention has grown toward the potential effects of electromagnetic fields (EMFs) on human health. Numerous scientific studies—both epidemiological and experimental—have led to the establishment of exposure limits, differentiated for the general public and workers, with the aim of preventing harmful effects. These limits have been incorporated into Italian regulations, including the Decree of the President of the Council of Ministers (DPCM) of 8 July 2003 [1], which is stricter than the guidelines of the International Commission on Non-Ionizing Radiation Protection (ICNIRP) [2]. At the international level, the issue is addressed through heterogeneous regulatory approaches, resulting in differing exposure limits for both the general population and workers.

Despite clear regulatory references and detailed technical guidelines for overhead power lines [3] [4] [5] [6], stationary electrical infrastructures - such as HV substations - present significantly more limited technical and regulatory documentation [7].

Compliance with these limits has become an essential requirement in the design, upgrading and management of electrical infrastructures. This creates the need for reliable tools to assess the intensity and distribution of electromagnetic fields generated by such installations. EMF assessment is not only a regulatory issue but also a fundamental component of environmental sustainability and plant safety [8] [9] [10].

In this scenario, there is growing interest in developing calculation methodologies that allow for effective evaluation while remaining compatible with technical design requirements. Electromagnetic analysis can indeed serve as a valuable decision-support tool, not only for regulatory compliance verification but also to guide design choices aimed at minimizing environmental impact and improving safety near electrical installations.

This thesis stems from this need and addresses the topic with a multidisciplinary approach, integrating physical principles, numerical modeling techniques and attention to regulatory and application aspects. The following chapters will detail the methods adopted and results obtained, with the aim of providing a useful and concrete contribution to electromagnetically-aware design of electrical installations.

1.1 Historical Background

The understanding of electromagnetic fields developed progressively from the 19th century, thanks to fundamental contributions by scientists like Hans Christian Ørsted, who demonstrated the connection between electricity and magnetism by observing the deflection of a magnetic needle near a current-carrying wire (1820). Subsequent experiments by Michael Faraday on electromagnetic induction (1831) and André-Marie Ampère's laws on forces between electric currents completed the initial framework, culminating in James Clerk Maxwell's theoretical synthesis. His equations (1861-1865) unified the phenomena of electricity, magnetism and light, demonstrating their propagation as electromagnetic waves at the speed of light. Heinrich Hertz later experimentally confirmed the existence of these waves, definitively validating Maxwell's theories. These equations represent the theoretical foundation for many technological innovations.

The second half of the 19th century, during the height of the Second Industrial Revolution, saw the transformation of theoretical discoveries into practical applications of great significance. This period witnessed the construction of the first urban electrical networks (Pearl Street Station in New York, 1882), the invention of the light bulb (Edison, 1879) and alternating current motors (Tesla, 1888). These developments led to profound changes in industrial production and electromagnetism transitioned from a purely physical phenomenon to becoming part of everyday life, marking the first widespread human exposure to artificial electromagnetic fields.

With the advent of large-scale electrification and modern technologies, interest in electromagnetic fields expanded to include biomedical engineering and medicine to evaluate exposure effects on the human body. This led to the establishment of safety thresholds by international (ICNIRP, WHO) and national regulatory bodies.

1.2 Theoretical Background

1.2.1 Maxwell's Equations

Electromagnetic fields are described by Maxwell's equations, which unify electrical and magnetic phenomena into a single theoretical framework. The equations in vacuum are presented below:

- Gauss's law for electric fields

$$\nabla \cdot \mathbf{E} = \frac{\rho}{\varepsilon_0} \tag{1.1}$$

- Gauss's law for magnetic fields

$$\nabla \cdot \mathbf{B} = 0 \tag{1.2}$$

- Faraday-Neumann-Lenz law

$$\nabla \times \mathbf{E} = -\frac{\partial \mathbf{B}}{\partial t} \tag{1.3}$$

- Ampère-Maxwell law

$$\nabla \times \mathbf{B} = \mu_0 \mathbf{J} + \mu_0 \varepsilon_0 \frac{\partial \mathbf{E}}{\partial t} \tag{1.4}$$

1.2.2 Electromagnetic Waves

From Maxwell's equations, in the absence of charges ($\rho = 0\,\mathrm{C/m^3}$) and currents ($\mathbf{J} = 0\,\mathrm{A/m^2}$), we derive the d'Alembert wave equation, which in its general form for any function $u(x, y, z, t)$ is:

$$\nabla^2 u - \frac{1}{v^2} \frac{\partial^2 u}{\partial t^2} = 0 \tag{1.5}$$

Taking the curl of the Faraday-Neumann-Lenz law 1.3:

$$\nabla \times (\nabla \times \mathbf{E}) = -\frac{\partial}{\partial t} (\nabla \times \mathbf{B}) \tag{1.6}$$

Applying the vector triple product identity to the left-hand side yields:

$$\nabla \times (\nabla \times \mathbf{E}) = \nabla(\nabla \cdot \mathbf{E}) - \nabla^2 \mathbf{E} \tag{1.7}$$

Since $\nabla \cdot \mathbf{E} = 0$ in the absence of charges according to Gauss's law for electric fields (1.1), we have:

$$\nabla \times (\nabla \times \mathbf{E}) = -\nabla^2 \mathbf{E} \tag{1.8}$$

Meanwhile, the right-hand term is computed using the Ampère-Maxwell law (1.4) in the absence of currents:

$$-\frac{\partial}{\partial t}(\nabla \times \mathbf{B}) = -\mu_0 \varepsilon_0 \frac{\partial^2 \mathbf{E}}{\partial t^2} \tag{1.9}$$

Substituting into 1.6 we obtain:

$$\nabla^2 \mathbf{E} - \mu_0 \varepsilon_0 \frac{\partial^2 \mathbf{E}}{\partial t^2} = 0 \tag{1.10}$$

Similarly, by taking the curl of the Ampère-Maxwell law (1.4), we obtain:

$$\nabla^2 \mathbf{B} - \mu_0 \varepsilon_0 \frac{\partial^2 \mathbf{B}}{\partial t^2} = 0. \tag{1.11}$$

The propagation velocity of electromagnetic waves is therefore $c = \frac{1}{\mu_0 \varepsilon_0} = \lambda f$. We can classify electromagnetic waves by frequency, with particular focus on the objectives of this work:

- **Low frequency waves ($1\,\text{Hz} - 100\,\text{kHz}$)** [2]
  Characteristic of power systems (50/60 Hz), where the *quasi-static approximation* can be applied to study electric and magnetic fields separately [11];
- **High frequency waves ($100\,\text{kHz} - 300\,\text{GHz}$)** [12]
  Used in telecommunications (e.g. radio signals, Wi-Fi). The *quasi-static approximation* no longer holds, though these remain non-ionizing;
- **Ionizing radiation ($f > 2 \times 10^{15}\,\text{Hz}$)** [13]
  Includes part of the ultraviolet spectrum, X-rays and gamma rays. These are ionizing as they possess sufficient energy to remove electrons from atoms, causing direct damage to DNA and tissues;

This work will primarily analyze low frequency waves.

1.2.3 Quasi-Static Approximation

The quasi-static approximation is fundamental for analyzing electrical circuits at power frequencies (50 Hz or 60 Hz). This approach simplifies the study of electromagnetic phenomena in power systems, avoiding the need to use the complete Maxwell's equations.

An electrical system operates under quasi-static conditions when its physical dimensions are much smaller than the wavelength associated with the operating frequency:

$$L \ll \lambda = \frac{c}{f} \tag{1.12}$$

For the European grid ($f = 50\,\text{Hz}$), $\lambda \approx 6000\,\text{km}$. This means the propagation time $\tau = L/c$ is so small that wave effects (phase delays and reflections) can be neglected.

Under these conditions, Maxwell's equations 1.3 and 1.4 can be rewritten neglecting their time dependence:

$$\nabla \times \mathbf{E} = -\frac{\partial \mathbf{B}}{\partial t} \approx 0, \qquad \nabla \times \mathbf{B} = \mu_0 \mathbf{J} + \mu_0 \varepsilon_0 \frac{\partial \mathbf{E}}{\partial t} \approx \mu_0 \mathbf{J} \tag{1.13}$$

These simplified equations show that the interactions between the electric field $\mathbf{E}$ and magnetic field $\mathbf{B}$ become negligible, allowing them to be studied separately. In particular, the electric field $\mathbf{E}$ becomes conservative and can be expressed as the gradient of a scalar potential as in electrostatics ($\mathbf{E} = -\nabla V$); while the magnetic field $\mathbf{B}$ depends exclusively on the current density $\mathbf{J}$ and can be calculated using the Biot-Savart law:

$$\mathbf{B}(\mathbf{r}) = \frac{\mu_0}{4\pi} \int \frac{\mathbf{J} \times \hat{r}}{r^2} dV \tag{1.14}$$

The quasi-static approximation ceases to be valid when the system's physical dimensions become comparable to the wavelength, as occurs in extensive high-voltage (HV) transmission lines. In such cases, propagation effects must be considered using distributed parameter models.

Conversely, the quasi-static approximation is perfectly applicable to electrical substations, switchgear, and - in general - all systems where dimensions are much smaller than λ. In this context, the study of electromagnetic phenomena can be significantly simplified by treating electric and magnetic fields separately.

Chapter 2

Effects of Electric and Magnetic Fields on the Human Body

Exposure to electric and magnetic fields is a topic of growing interest, particularly following the expansion of power networks. The human body, composed primarily of conductive tissues, can interact with these fields in ways that depend on frequency, intensity and exposure duration. This chapter examines known and presumed effects of EMFs on human health, distinguishing between acute and chronic effects, between low- and high-frequency fields.

2.1 Ionizing and Non-Ionizing Radiation

Electromagnetic radiation is classified as ionizing or non-ionizing based on its energy. Planck's law establishes a direct relationship between energy and frequency:

$$E = h \cdot f \tag{2.1}$$

where E is the photon energy, $h \approx 6.626 \times 10^{-34}$ J is Planck's constant and f is the wave frequency. When energy E is sufficient to overcome electron binding energy in atoms, the radiation is considered ionizing. Exposure to this type of radiation can cause irreversible damage to cellular structures - particularly DNA - with biological effects that persist even after exposure ends (e.g. genetic mutations). According to the Federal Communications Commission (FCC), radiation with energy exceeding 10 eV [13] is considered ionizing, corresponding to frequencies above 2.4×10^{15} Hz.

The frequencies used in electrical systems and telecommunications are much lower, making the corresponding radiation non-ionizing. Although incapable of

directly ionizing matter, they can still interact with biological tissues. The most common effects, such as localized tissue heating, are generally transient and resolve upon cessation of exposure. Effects from prolonged or repeated exposure remain subjects of ongoing research and scientific debate.

Due to these differences, separate regulations exist for protection against ionizing radiation (e.g. Legislative Decree 101/2020), governed by very restrictive criteria, and non-ionizing radiation (e.g. DPCM 8 July 2003). This study will focus on non-ionizing radiation.

2.2 Acute Effects of Non-Ionizing Fields

The interaction mechanism between electromagnetic fields and the human body depends strongly on frequency. The quasi-static approximation, considering the human body's typical scale of about one meter, remains applicable for frequencies below 100 kHz. Indeed, at 100 kHz the wavelength in vacuum is $\lambda \approx 3000\,\mathrm{m} \gg 1\,\mathrm{m}$, justifying the separate treatment of electric and magnetic fields. For higher frequencies, this approximation becomes invalid and the phenomena must be described collectively.

Another crucial factor is the frequency-dependent electrical properties of human tissue, as illustrated in 2.1.

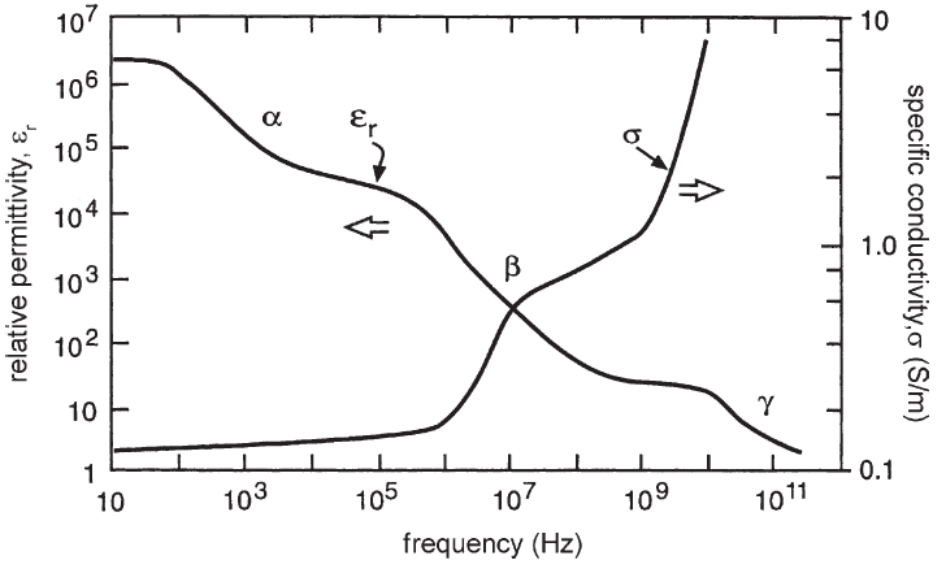

Figure 2.1: Typical frequency dependence of the complex permittivity of heterogeneous materials like biological tissues [14].

2.2.1 Low Frequency Electromagnetic Fields

Electric field

Electric fields interact with the conductive human body by inducing a charge distribution on the skin surface. This surface polarization creates a partial shielding effect that drastically reduces the electric field intensity inside the body.

The distribution of induced charges and currents is not uniform. It depends on the body's position in the field, its shape and size, as well as exposure conditions.

This can be easily observed using simplified models (e.g. homogeneous sphere), which show that the internally induced electric field intensity is proportional to the external field E_0 and its frequency and inversely proportional to the tissue conductivity σ. The relationship, valid in the low-frequency regime, can be approximated as:

$$E_{int} \approx \frac{3\varepsilon_0\omega}{\sigma} E_0 \tag{2.2}$$

This implies that an external field of 1 kV/m at power frequency can generate inside the body a field of just a few mV/m, representing a reduction of several orders of magnitude. [15].

This attenuation is influenced by the electrical properties of tissues, particularly by conductivity, which governs current flow, and by permittivity, which determines the degree of polarization. Both vary across different tissues and are functions of the applied field frequency.

At the cellular level, the electric field effect is further mitigated. Considering a spherical cell immersed in tissue exposed to the field, the induced membrane potential variation is proportional to the product of the local field and the cell radius r:

$$V_m \approx 1{,}5 r E_{loc} \tag{2.3}$$

For typical cellular dimensions, an internal electric field $E_{loc} = 1\,\text{mV/m}$ results in induced membrane potentials on the order of 10 nV. In the case of elongated cells (i.e. axons), particularly when aligned parallel to the field, higher values up to approximately 10 μV are obtained. The induced quantities in deep tissues remain below levels considered physiologically active [15].

At the surface level, however, current can be generated and it may stimulate cutaneous nerve endings and superficial muscles, causing perceptible sensations such as tingling and involuntary contractions.

Direct perception of electric fields occurs at intensities between 2 and 5 kV/m, while discomfort becomes significant between 15 and 20 kV/m [2].

Magnetic Field

The relative magnetic permeability of the human body is $\mu_r \approx 1$, therefore the magnetic field penetrates the human body unobstructed, inducing currents within the body according to Faraday-Neumann-Lenz's law (1.3).

This induced electric field gives rise to circulating electric currents in the conductive tissues of the body. The intensity of the induced field and the resulting current density depend on several factors: local electrical conductivity, rate of change of the magnetic field, and the size of closed loops (circuits) along which the field acts. In general, larger body regions tend to exhibit higher induced electric fields. These currents, if sufficiently high, can directly stimulate the nervous or muscular system, causing involuntary contractions, tingling, dizziness and nausea.

The actual distribution of induced currents in the body strongly depends on anatomical heterogeneity and spatial variability of tissue electrical properties. To accurately estimate current density, advanced computational models, based on realistic body geometries and high-resolution numerical methods, are employed.

The induced currents, if sufficiently strong, can stimulate the nervous and muscular system causing involuntary contractions, tingling, dizziness or nausea. A well-documented physiological effect in human literature is the perception of magnetic phosphenes, visual sensations caused by currents induced in the retina. This effect is often used as a reference for exposure limit definitions.

Figure 2.2 shows the magnetic flux density thresholds (as a function of frequency) required to excite various excitable tissues: central and peripheral nerve fibers, cardiac tissue and retina. The figure compares these threshold values with exposure limits established by ICNIRP and IEEE guidelines. The data were calculated based on models proposed by Reilly [14] and reported by Foster [15].

2.2.2 High Frequency Electromagnetic Fields

The interaction of electromagnetic fields with the human body is dominated by energy absorption phenomena, particularly through ohmic heating of tissues.

For this reason, the quantity used to measure the effects is the Specific Absorption Rate (SAR). SAR is the power absorbed per unit of body mass and it is measured in W/kg. It is used to evaluate tissue heating when exposed to electromagnetic fields.

Water molecules, abundant in the human body, move following the alternation of high-frequency electric fields, generating heat. However, energy absorption becomes significant only at frequencies above approximately 100 kHz, while at lower frequencies the absorbed energy is negligible and does not cause measurable body heating.

The penetration depth decreases with increasing frequency, according to the skin effect law. This phenomenon describes the tendency of currents to concentrate

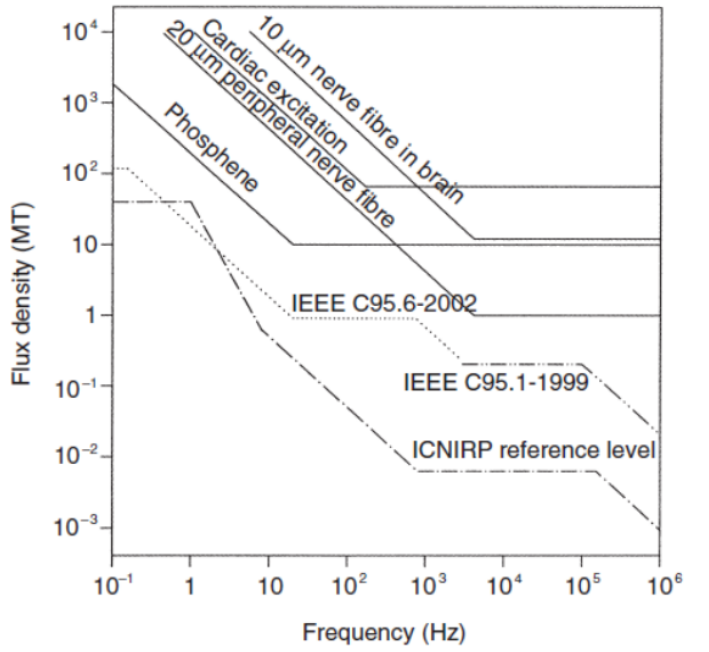

Figure 2.2: Excitation thresholds for different physiological phenomena as a function of frequency, expressed in terms of magnetic flux density [15].

in surface layers of a conductor exposed to time-varying fields. The penetration depth δ can be estimated with the relation:

$$\delta = \sqrt{\frac{2}{\mu\sigma\omega}} \tag{2.4}$$

where μ is the magnetic permeability of the tissue, and σ is its electrical conductivity. At frequencies above 10 GHz, the penetration depth is greatly reduced, and energy is absorbed almost exclusively in the superficial skin layers. The effects are more pronounced in poorly vascularized tissues (e.g. eyes and testicles) which dissipate heat less efficiently [16].

In the 100 kHz to 10 GHz range, the distribution of absorbed energy is highly non-uniform and depends on multiple factors: field intensity, frequency, polarization, body geometry and dielectric properties of tissues.

At intermediate frequencies (100 kHz - 1 MHz), a transition occurs: the interaction is dominated by both resistive effects (induced currents) and dielectric effects (absorption and heating).

2.3 Chronic Effects of Non-Ionizing Electromagnetic Fields

The potential chronic effects resulting from prolonged or repeated exposure to magnetic fields remain subject to debate and ongoing research in the scientific community. Unlike acute effects, which manifest during or immediately after exposure, chronic effects may emerge after extended periods. To date, various studies have yielded conflicting results.

In light of this, in 2002, the International Agency for Research on Cancer (IARC) classified low-frequency magnetic fields as possibly carcinogenic to humans (Group 2B). This classification is based on "limited evidence" of carcinogenicity in humans (childhood leukemia) and "inadequate" evidence in laboratory animals. The decision reflects a balance between statistical evidence and the absence of a clearly identified biological mechanism [15].

It should be noted that IARC classifies substances into 4 groups:

- Group 1 - Carcinogenic to humans
  Sufficient evidence that the agent causes cancer in humans
- Group 2A - Probably carcinogenic to humans
  Limited evidence in humans but sufficient in animals
- Group 2B - Possibly carcinogenic to humans
  Limited evidence in both humans and animals
- Group 3 - Not classifiable as to carcinogenicity
  Inadequate evidence in humans and animals
- Group 4 - Probably not carcinogenic to humans
  Evidence that the agent is not carcinogenic

It must be emphasized that, to date, there is no definitive scientific consensus on the actual chronic hazards of low-frequency magnetic fields. We will now examine the main epidemiological evidence.

2.3.1 Children

One of the most well-known studies in the field is the research conducted by Wertheimer and Leeper (1979) [17], who were the first to hypothesize an association between power-frequency electromagnetic fields and the onset of childhood leukemia. The study did not demonstrate a causal relationship but was the first to raise the hypothesis that chronic exposure to electromagnetic fields could have adverse health effects. Although this work had several limitations – including the absence

of direct measurements and the possible influence of confounding factors such as socioeconomic status – it generated significant interest within the scientific community and the general public.

Among these, the study coordinated by Anders Ahlbom (2000) [18] is a meta-analysis commissioned by the World Health Organization (WHO) and published in the British Journal of Cancer. The work synthesized the results of numerous epidemiological studies on the association between chronic exposure to low-frequency magnetic fields and the risk of childhood leukemia. In this context, they examined data from 9 case-control studies conducted in various countries, including only those with direct measurements of magnetic fields in homes. The analysis showed that for exposures above 0.4 μT, the relative risk of childhood leukemia was higher compared to children exposed to levels below 0.1 μT. However, only a small percentage of children fell within the high exposure range ($< 1\,\%$). The study concluded that there was a weak but consistent association between exposure to power-frequency magnetic fields and childhood leukemia, though not sufficient to establish a causal relationship.

Subsequently, Kheifets et al. (2010) [19] conducted a systematic and updated review of epidemiological studies carried out after Ahlbom's (2000) meta-analysis to verify whether new studies published in the following decade confirmed or contradicted those results. The study reaffirmed the existence of a weak association between magnetic field exposure and childhood leukemia. Moreover, the possible role of bias or unmeasured confounding factors, such as socioeconomic or environmental conditions, was not excluded. Also in this case, only a small percentage of children fell into the high exposure range ($< 1\,\%$) and it was repeated that there is no direct experimental evidence of a biological mechanism through which such low-intensity fields could induce cellular or genetic alterations.

One of the most recent and comprehensive analyses is by Seomun et al. (2021) [20]. The results show that for exposures $B \geq 0.4\,\mu$T, the risk of childhood leukemia increases. For other tumors, such as brain cancers, the association is not significant.

However, not all studies confirm the association between ELF magnetic field exposure and childhood leukemia. For example, the study by Amoon et al. (2022) [21] did not find any statistically significant correlation. The authors of the study propose several possible explanations for this change. It could simply be a chance effect in the early studies or undetected methodological biases.

Although some studies have shown a statistical association, this evidence remains insufficient to draw definitive conclusions. This is due to the fact that no plausible biological mechanism is known through which such fields could cause cellular or genetic alterations, nor is a possible dose-effect relationship clear, which is a crucial element for defining such a link. In light of these uncertainties, it is essential to continue research to clarify the health risks.

2.3.2 Pregnant Women

Epidemiological research on pregnancy outcomes has not revealed solid evidence of adverse reproductive effects in women using video display terminals for professional purposes [22]. Specifically, the meta-analysis by Shaw et al. (1993) aggregated several comparative studies between pregnant women exposed and unexposed to video terminal use, showing no increased risk of spontaneous abortion or congenital anomalies [23]. The investigation by Bracken et al. (1995) [24] concluded that neither birth weight nor fetal growth were affected by ELF field exposure. Furthermore, no association was observed between high exposure levels and delivery complications.

Overall, available evidence does not support the hypothesis of a link between occupational video terminal use and reproductive health effects [25].

2.3.3 Adult Workers

Regarding adults, epidemiological evidence appears less consistent compared to children. Savitz et al. (1998) [26] conducted a cohort study of over 138,000 electrical utility workers in the United States, observing a modest increased risk of brain tumors (particularly gliomas) and neuro degenerative diseases, such as Alzheimer's disease and ALS (amyotrophic lateral sclerosis), in subjects occupationally exposed to above-average magnetic fields. The observed effect was more pronounced for prolonged exposure periods.

However, subsequent studies have yielded conflicting results. For instance, Johansen et al. (2000) [27] analyzed a large sample of Danish electrical industry workers, finding no significant evidence of increased risk of brain tumors or leukemias. Similarly, Håkansson et al. (2003) [28], in a Swedish study of over 500,000 workers, observed no consistent association between occupational exposure to power-frequency magnetic fields and increased oncological or neuro degenerative risk.

These discrepancies reflect the inherent methodological challenges in such studies, including retrospective exposure assessment, potential selection bias and heterogeneity of working conditions. In the absence of a clear biological mechanism linking power-frequency magnetic fields to neuro degenerative or oncogenic processes, current evidence does not establish a causal relationship in adults.

2.4 Regulations and Guidelines

Human exposure to electromagnetic fields is regulated internationally by various organizations, which establish limits based on scientific evidence and potential health risks.

2.4.1 ICNIRP

The main international body is the International Commission on Non-Ionizing Radiation Protection (ICNIRP). It is an independent and non-profit scientific organization recognized by the World Health Organization (WHO). The primary objective of ICNIRP is to protect human health by defining exposure limits to non-ionizing fields based exclusively on scientific criteria. The Commission operates through a systematic and rigorous review of international scientific literature, assessing known and potentially harmful biological effects.

ICNIRP distinguishes two main categories of exposed individuals:

- General public: includes all individuals, including vulnerable groups. More restrictive limits are applied.
- Occupationally exposed workers: healthy individuals, trained and aware of the exposure.

The ICNIRP guidelines concerning exposure to low-frequency electric and magnetic fields (2010) [2] are based on established biological effects, namely the acute effects of fields (induction of currents in human body tissues). These currents may interfere with the normal functioning of the nervous, muscular and cardiac systems. ICNIRP has established exposure limits to prevent the stimulation thresholds of excitable tissues, such as nerves and muscles, from being exceeded. The basic restrictions defined by the guidelines are reported in Table 2.1.

	General Public	**Workers**
Internal electric field (E)	200 mV/m	100 mV/m

Table 2.1: ICNIRP basic restrictions (RMS values) for exposure to low-frequency electromagnetic fields (50 Hz)

Since internal quantities cannot be directly measured, ICNIRP also provides reference levels for electric field and magnetic flux density, which are directly measurable, as shown in Table 2.2. These reference levels are calculated to ensure that the basic restrictions are not exceeded, even in the worst-case scenario.

	General Public	**Workers**
Magnetic flux density (B)	200 μT	1000 μT
Electric field (E)	5 kV/m	10 kV/m

Table 2.2: ICNIRP reference levels (RMS values) for exposure to low-frequency electromagnetic fields (50 Hz)

The World Health Organization (WHO), through the International EMF Project, recognizes the ICNIRP guidelines as the technical-scientific reference for public health protection. Although the WHO does not have direct regulatory authority, it recommends that national legislation be inspired by these guidelines, thereby ensuring a consistent approach to the protection of both the public and workers.

ICNIRP also defines exposure limits for high-frequency electromagnetic fields; however, these aspects will not be addressed here, as they fall outside the scope of this thesis.

2.4.2 European Union

The European Union has issued specific regulatory documents to protect the public and workers from exposure to electromagnetic fields, in line with scientific evidence and international guidelines, particularly those of the ICNIRP.

Recommendation 1999/519/EC – Protection of the General Public

Council Recommendation 1999/519/EC [29] establishes exposure limits to electromagnetic fields for the general public. It is non-binding, but serves as a regulatory reference adopted by most Member States. The recommended limits are 100 μT and 5 kV/m.

Directive 2013/35/EU – Protection of Workers

Directive 2013/35/EU [30] regulates the protection of workers from risks related to exposure to electromagnetic fields in the workplace. It is mandatory for Member States, which must implement it into national legislation.

The directive defines exposure limits based on ICNIRP guidelines and considers only acute and confirmed effects of electromagnetic field exposure. Therefore, potential chronic effects (e.g. cancer, Alzheimer's disease) are not taken into account, as they are not yet scientifically confirmed.

The directive distinguishes the effects of field exposure based on severity: health effects and sensory effects. Health effects represent a risk to health and must always

be avoided. At 50 Hz, these include:

- Direct stimulation of the nervous and muscular systems
- Involuntary muscle contractions
- Cardiac arrhythmia (in extreme cases)

Sensory effects are milder, and the associated emission limits may be temporarily exceeded if they do not pose safety risks. These include:

- Dizziness, nausea
- Tingling or vibration sensations on the skin
- Difficulty concentrating or balance disturbances

The exposure limit values (ELVs) are expressed as peak values of internal electric field within the human body. At 50 Hz, the ELVs are shown in Table 2.3.

	Health Effects	**Sensory Effects**
Internal electric field	1.1 V/m	0.14 V/m

Table 2.3: Peak ELVs for workers' exposure to low-frequency electromagnetic fields (50 Hz)

The directive also defines Action Levels (ALs), expressed in terms of external electric field and magnetic flux density, to simplify exposure assessment. Two levels are defined: lower AL and upper AL.

For the magnetic field, compliance with the lower AL ensures compliance with the ELV for sensory effects, while compliance with the upper AL ensures compliance with the ELV for health effects.

For the electric field, both action levels ensure compliance with the ELV for sensory effects; however, if the upper AL is exceeded, additional protective measures must be implemented, such as equipotential bonding between workers and work objects, as indicated by the directive.

The AL values at 50 Hz are shown in Table 2.4.

	Lower AL	**Upper AL**
Magnetic flux density (B)	1 mT	6 mT
Electric field (E)	10 kV/m	20 kV/m

Table 2.4: Action Levels (RMS values) for workers' exposure to low-frequency electromagnetic fields (50 Hz)

If the lower AL is exceeded, it must be verified that the ELV is still respected. In such a case, no further safety measures are required.

2.4.3 Italy

Framework Law No. 36/2001 – Protection from Exposure to Electromagnetic Fields

In Italy, the protection of the public from exposure to electric and magnetic fields is governed by Law No. 36 of 22 February 2001, known as the Framework Law on Protection from Exposure to Electromagnetic Fields [31]. This law constitutes the national regulatory foundation for managing non-occupational exposure risks, with particular attention to power lines, telecommunications and broadcasting systems.

The law is based on several key principles:

- **Precautionary principle:** even in the absence of conclusive evidence of harmful effects, precautionary measures must be taken to minimize exposure;
- **Protection of human health:** the right of citizens to live in a healthy environment is recognized, even in the presence of scientific uncertainty regarding long-term effects from low-intensity exposure;
- **Information and participation:** citizens have the right to be informed about electromagnetic field exposure and to participate in authorization procedures.

The law introduces three core concepts for exposure control:

- **Exposure limit:** the level of electromagnetic field that must not be exceeded under any circumstances, in order to prevent acute and scientifically confirmed effects;
- **Attention value:** a more precautionary level intended to reduce the risk of long-term effects, even if not scientifically proven, particularly for prolonged exposure in sensitive environments (e.g. homes, schools);
- **Quality objective:** non-binding parameters to be considered in urban planning and infrastructure design, aimed at promoting overall exposure minimization.

These values are not set directly by the law, but are defined through implementing decrees based on technical-scientific criteria, taking into account international recommendations as well as specific national conditions.

The law assigns the State the responsibility of establishing general criteria and ensuring regulatory consistency throughout the country. Regions and autonomous provinces hold legislative and administrative powers at the local level, while municipalities are involved in urban planning and issuing permits for installations. Regional Environmental Protection Agencies (ARPAs) carry out monitoring, control, and technical support activities.

DPCM of 8 July 2003 – Limits and Criteria for Power Installations

The Decree of the President of the Council of Ministers (DPCM) of 8 July 2003 is the main implementing regulation of Framework Law No. 36/2001 concerning installations for the transmission, distribution, and transformation of electrical energy at 50 Hz [1]. This decree establishes the RMS values for exposure limits, attention values and quality objectives, in accordance with the principles set forth in the framework law.

It applies to medium and high-voltage (MV and HV) electrical infrastructures.

- **Exposure limit:**
  - Electric field: 5 kV/m
  - Magnetic induction: 100 μT
- **Attention value:**
  - Magnetic induction: 10 μT
- **Quality objective:**
  - Magnetic induction: 3 μT

The exposure limit is an instantaneous value that must never be exceeded, whereas the attention value and quality objective refer to the 24-hour average.

Italy adopts significantly more stringent limits for magnetic induction compared to international standards. This reflects a precautionary approach, motivated by long-term scientific uncertainties and the need to protect public health, especially in areas where people may remain for extended periods such as homes, schools and hospitals.

Legislative Decree 81/2008 – Consolidated Act on Occupational Safety

The Italian regulation governing workers' exposure to electromagnetic fields falls within the broader framework of occupational health and safety, as set forth by Legislative Decree No. 81/2008 (also known as the "Consolidated Act on Occupational Safety") [32]. Specifically, Title VIII, Chapter IV of the decree fully implements European Directive 2013/35/EU, which sets minimum requirements for the protection of workers from risks arising from exposure to electromagnetic fields.

While Italy adopts more restrictive limits for the general population to account for potential long-term effects not yet confirmed, it follows the internationally defined limits for workers, which consider only acute and scientifically established effects.

Chapter 3

Electrical Substations

High-Voltage electrical substations represent fundamental nodes in the transmission network. Their primary function is to transform voltage levels and route electrical energy coming from high-voltage transmission lines to lower voltage levels, compatible with local distribution. We refer to an electrical substation when at least one of the interconnected systems belongs to category III, meaning with voltage exceeding 30 kV.

In these substations, the transformer plays a central role in connecting two different voltage levels, acting as a node between the respective power lines. The substation is also equipped with all necessary devices for operational maneuvers, such as opening, closing and sectioning circuits, as well as managing power flows and protecting the installation.

Since they are located upstream of the distribution network, these infrastructures play a strategic role in ensuring system reliability: high service continuity is therefore required to avoid interruptions in power supply. The design and configuration of these substations influence not only the technical and economic performance of the network but also the characteristics of the generated electric and magnetic fields, with implications for human safety.

This chapter will analyze the structure of substations for the purpose of proper modeling for electric and magnetic field analysis.

3.1 Voltage Levels

The European harmonized standard CEI EN 60038 [33] defines alternating voltage levels and their respective categories:

- **Category I – Low Voltage (LV)**: $V_n \leq 1\,\text{kV}$ (e.g. 230 V, 400 V)
- **Category II – Medium Voltage (MV)**: $1\,\text{kV} < V_n \leq 30\,\text{kV}$ (e.g. 15 kV, 20 kV)
- **Category III – High Voltage (HV)**: $V_n > 30\,\text{kV}$

In practice, category III is further divided into High Voltage (HV) for the range $30\,\text{kV} < V_n \leq 150\,\text{kV}$ and **Extra High Voltage (EHV)** for $V_n > 150\,\text{kV}$.

The Italian national power grid can be divided into a transmission network operating at nominal voltages of 220 kV and 380 kV, and a sub-transmission network operating at nominal voltages of 132 kV and 150 kV. Based on the operating voltage level, electrical substations are classified as **Primary substation** EHV/HV (e.g. 220 kV/150 kV) and **Secondary substation (or primary distribution substation)** HV/MV (e.g. 132 kV/20 kV). The terminology may vary depending on whether referring to the transmission or distribution network. In fact, an HV/MV substation is considered the second in the transmission network and the first in the distribution network.

The MV distribution network features multiple nominal operating voltage levels. The most common are:

- **15 kV**: Piedmont, Lombardy, Liguria, Emilia-Romagna, Tuscany, Sardinia, Lazio;
- **20 kV**: Veneto, Trentino-Alto Adige, Puglia, Campania, Sicily.

3.2 Busbar Configurations

The reliability of an electrical substation is influenced by several factors, including the arrangement of switching devices and busbars. This defines the station's geometry and consequently affects the emission of electric and magnetic fields. The six most common configurations are:

1. Single busbar
2. Main and transfer busbar
3. Double busbar with single breaker

4. Double busbar with double breaker
5. Ring busbar
6. Breaker-and-a-half configuration

This section will analyze these six basic configurations along with their advantages and disadvantages.

3.2.1 Single Busbar

This is the simplest arrangement, where all connections are linked to a single busbar, as shown in Figure 3.1.

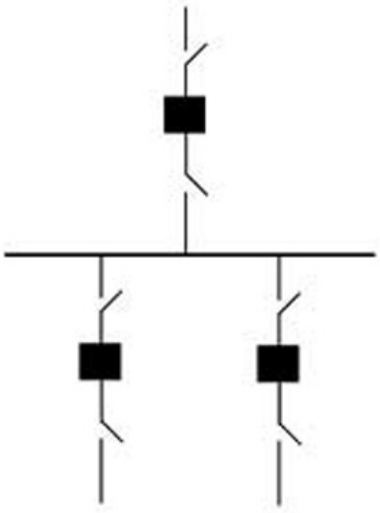

Figure 3.1: Single busbar configuration

This configuration lacks redundancy, resulting in low overall reliability. In case of a fault on the main busbar will cause the entire substation to shut down. For maintenance of switching devices, the affected line must be disconnected, while work on the busbar requires de-energizing the entire substation. This configuration has low costs but also limited operational flexibility. Due to its poor reliability, maintenance challenges, and operational rigidity, this arrangement is only suitable for installations with small loads and modest availability requirements. Often, the single busbar represents only the initial development phase of a substation. Therefore, design must account for possible future expansions, such as adding power lines, transformers, or busbar sections.

3.2.2 Main and Transfer Busbar

Circuits are connected between a main busbar and a transfer busbar, as shown in Figure 3.2.

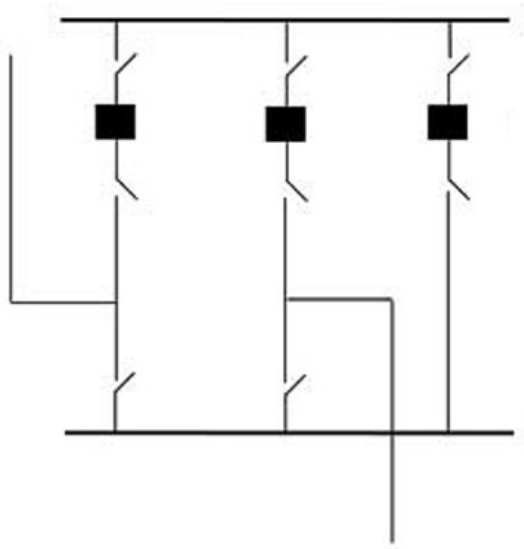

Figure 3.2: Main and transfer busbar configuration

Under normal conditions, all circuits are connected to the main busbar, resulting in limited operational reliability: a fault on the main busbar deactivates the entire plant. However, the transfer busbar facilitates maintenance: if a breaker requires servicing, the circuit load can be transferred to the transfer busbar via the tie breaker, avoiding service interruption. This configuration requires an additional breaker - called a bus tie breaker - which directly connects the main and transfer busbars.

Another operational advantage is the ability to deactivate the main busbar without interrupting circuit supply, as they can be temporarily served by the transfer busbar. However, it should be noted that when the main busbar system is out of service, there remains no direct protection breaker for the lines, increasing the risk of total service loss in case of faults. In summary, this configuration is suitable for plants with modest reliability requirements and low operational complexity. Despite its low cost and widespread use, it doesn't always guarantee high levels of flexibility and reliability.

3.2.3 Double Busbar with Single Breaker

In this configuration, each circuit is connected to two busbars, with a tie breaker between them, as shown in Figure 3.3.

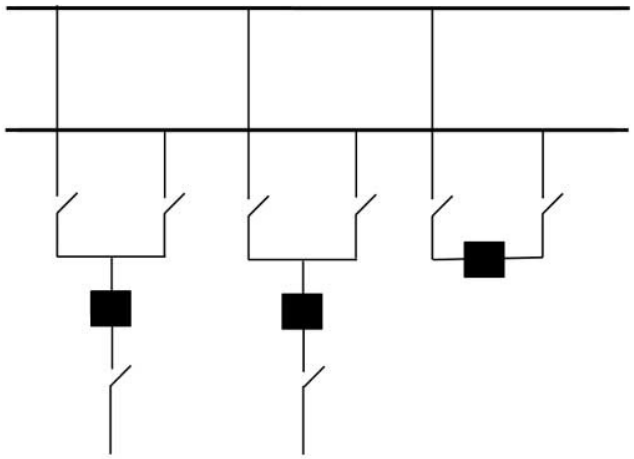

Figure 3.3: Double busbar with single breaker configuration

This configuration uses two switching disconnectors per line but only one breaker per circuit. The disconnectors allow transferring the line connection from one busbar to another without de-energizing it, by closing the bus tie breaker. If the system operates with the bus tie breaker closed, circuits can be fed from both busbars, offering greater operational flexibility and better system reliability: if one busbar fails, the other can still maintain active circuits. However, if the tie breaker is open, the two busbars operate completely independently and can no longer support each other. In this case, redundancy is lost and a fault on one busbar results in power interruption for its connected circuits.

Relay protection is complex due to the possibility of transferring circuits between busbars. Therefore, it's essential to establish rigorous operational procedures to ensure correct and safe configurations. A failure of the bus tie breaker would result in the shutdown of the entire substation, making it a critical element for the overall plant reliability.

From a maintenance perspective, the double busbar allows easier work on the busbars themselves without compromising service continuity. However, line breaker maintenance still requires circuit shutdown, similar to the single busbar configuration.

This solution is suitable where load transfers and higher operational reliability are required. However, due to its single-breaker-per-line structure, this configuration has limited reliability and is generally not recommended for highly critical substations.

3.2.4 Double Busbar with Double Breaker

In this configuration, each circuit is connected to two busbars and protected by two breakers, as shown in Figure 3.4. Thanks to redundancy, a fault on one busbar or circuit doesn't compromise the operation of other sections, ensuring high system reliability. In standard operation, each line is simultaneously connected to both busbars but it's also possible to distribute lines between the two systems, making the configuration flexible according to operational needs. In case of a fault on one system, the presence of double breakers allows rapid plant reconfiguration, limiting service disruption.

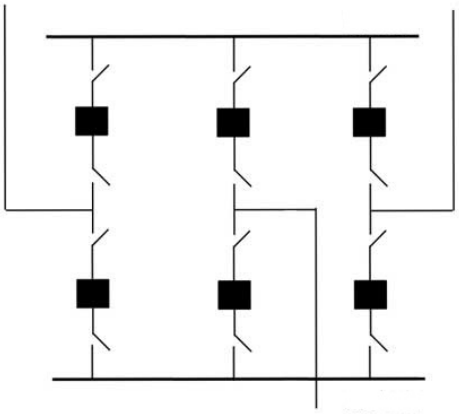

Figure 3.4: Double busbar with double breaker configuration

However, the double number of devices and busbars leads to significantly higher costs. Beyond greater initial investments, maintenance activities also become more complex and expensive. Careful consideration must also be given to the physical arrangement of busbars to avoid unwanted coupling phenomena between the two systems. Despite the apparent redundancy, the reliability increase isn't always proportional to the number of components, which is why adopting this configuration requires careful balancing based on the plant's specific needs. Beyond reliability, this configuration offers remarkable operational flexibility, allowing specific lines to be fed from a selected busbar section through appropriate switching. These characteristics make it ideal for loads requiring high service continuity and minimal interruption times.

3.2.5 Ring Busbar

In this arrangement, breakers are arranged in a ring, with circuits connected between two breakers, as shown in Figure 3.5.

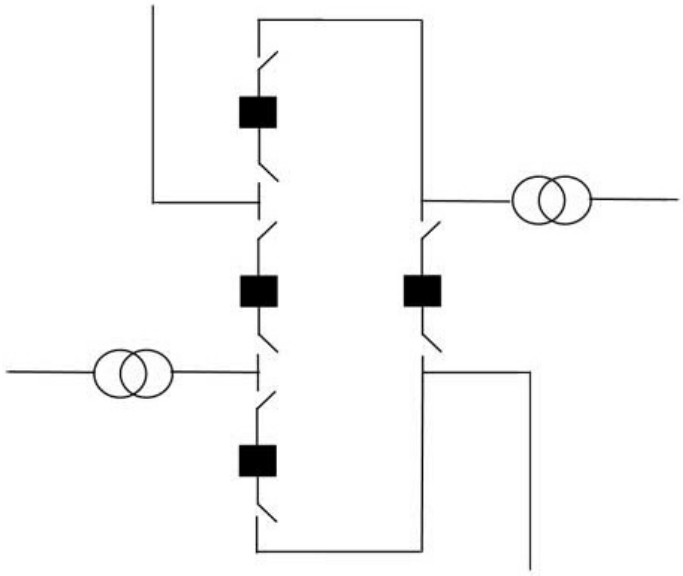

Figure 3.5: Ring busbar configuration

This configuration ensures high operational reliability: a fault on one busbar section only interrupts the affected circuit, while a circuit fault doesn't affect other operations. During normal operation, all breakers are closed. When a line fault occurs, the two nearest breakers intervene; if one or both fail, the next breaker activates, still ensuring selectivity.

Relay protection is more complex and may require more devices per circuit. Additionally, busbars and breakers must have the same current rating since current flow distribution varies according to the system's operational state. Protection activation and automatic reclosing require greater complexity compared to other configurations. However, no protection modifications are needed when transitioning between any possible ring configurations.

From a maintenance perspective, the ring busbar offers significant flexibility: a breaker can be serviced without interrupting the load, as the circuit's other breaker can remain in service. Similarly, a ring portion can be isolated for maintenance without compromising power supply to other circuits.

Costs are high as each circuit requires two breakers (though one may be shared between adjacent circuits). However, this solution remains relatively economical, reliable and flexible. This configuration is ideal for loads requiring high reliability

but has some disadvantages:

1. The failure of a single breaker can compromise the entire substation, depending on ring length and number of involved breakers;

2. Expandability is limited by the maximum number of circuits physically implementable in the ring;

3. To maintain balance and service continuity, it's essential to alternate supply and load circuits; having two adjacent supply circuits could leave the substation without power in case of a fault.

3.2.6 Breaker-and-a-Half Configuration

In this scheme, each circuit is protected by two breakers on a three-breaker line connected to two busbars, with a ratio of "one-and-a-half breakers" per circuit, as shown in Figure 3.6. This configuration allows load feeding through two busbars and ensures each circuit can remain in service during faults or maintenance operations.

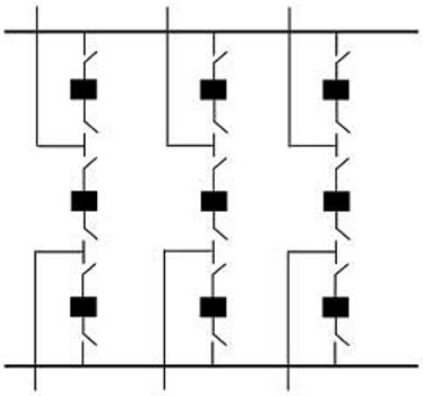

Figure 3.6: Breaker-and-a-half configuration

One of this scheme's main strengths is its high reliability: a circuit fault doesn't affect others, while a busbar fault doesn't impact load feeding. Under normal operation, all breakers are closed, with both busbars energized. When a line fault occurs, the two associated breakers intervene. If one fails, the next breaker activates.

Additionally, the configuration facilitates maintenance: an entire busbar and adjacent breakers can be serviced without causing service interruptions. Another advantage is remarkable expandability: with careful planning, new circuits can be

added while minimizing conflicts with external lines and maintaining operational consistency.

However, this solution has some disadvantages. The main one is physical space requirements: significant space is needed, especially in high-voltage installations where large safety distances between components must be maintained. Furthermore, relay protection is complex and expensive, requiring numerous devices and sophisticated coordination logic.

From an economic perspective, plant costs are proportional to the number of circuits, but justified by the good compromise between reliability, operational flexibility, safety and maintenance ease that this configuration offers.

3.3 Qualitative Analysis of Electric and Magnetic Fields

The magnetic field emission in electrical substations is strongly influenced by the geometry of conductors and the arrangement of currents. Different busbar configurations exhibit distinctive characteristics in terms of the generated electric and magnetic fields.

Regarding the electric field, in the case of a double busbar configuration compared to a single busbar, there is an additional source of the field (the second busbar at the same voltage and phase), leading to an increase in the generated electric field. In the main and transfer busbar arrangement, typically only one of the two busbars is energized at a time. Therefore, the resulting electric field is substantially equivalent to that produced by a single busbar. However, during switching operations, peaks in the electric field may be observed.

The resulting magnetic field near the busbars depends on the current intensities and the direction in which they flow. In configurations with two energized busbars, the respective generated fields may either sum or partially cancel each other, depending on the observer's position and the relative orientation of the conductors. In the ring configuration, the results depend on the feeding mode: if the current flows continuously along the entire perimeter (as in a loop), the magnetic field is concentrated inside the ring, with higher intensity compared to the outside. In such a case, the field tends to decay more rapidly externally, as the contributions from opposing conductors reinforce internally and partially cancel each other externally.

3.4 Gas-Insulated Substations (GIS)

A GIS uses a high-performance dielectric gas, sulfur hexafluoride (SF_6), for phase-to-phase and phase-to-ground insulation. High-voltage conductors, circuit breakers, disconnectors, current transformers (CTs), and voltage transformers (VTs) are enclosed within grounded metallic housings filled with SF_6 gas. While a conventional air-insulated substation (AIS) requires meters of spacing to ensure insulation, GIS achieves the same result in a much smaller space thanks to the properties of SF_6. Consequently, a GIS is more compact than an AIS.

This type of substation is particularly suitable for areas where space is limited or expensive. Moreover, since the active components are protected from exposure to atmospheric air, moisture, and external contaminants, GIS offers greater reliability, requires less maintenance and has a longer operational life (over 50 years) compared to AIS. [34]

3.4.1 Sulfur Hexafluoride (SF_6)

Sulfur hexafluoride (SF_6) is an inert, colorless, odorless, tasteless, non-toxic and non-flammable gas composed of one sulfur atom bonded to six fluorine atoms. SF_6 offers insulating capacity two to three times higher than air at the same pressure and is approximately one hundred times more effective in arc interruption.

This gas is widely used as an interrupting medium in high-voltage circuit breakers, replacing older oil- and air-based systems. In the presence of an arc or spark, SF_6 decomposes due to high temperatures, but most of the gas spontaneously recombines, minimizing the need for replenishment. However, small amounts of reactive by-products are formed due to the interaction of sulfur and fluorine ions with traces of moisture, air and other contaminants. These residues are neutralized over time by special molecular absorbing filters integrated into the GIS system.

SF_6 is a potent greenhouse gas, with a global warming potential thousands of times greater than CO_2 and it has an extremely long atmospheric lifetime (half-life of about 3200 years), making its cumulative impact significant and persistent. In the context of the ecological transition and the reduction of climate-altering emissions, Regulation (EU) 2024/573 [35] aims to phase out the use of fluorinated greenhouse gases, including sulfur hexafluoride (SF_6). Specifically, the regulation bans the commissioning of new medium-voltage switchgear containing SF_6 starting January 1, 2026 for equipment up to 24 kV, and from January 1, 2030 for equipment up to 52 kV. This regulation promotes the adoption of environmentally friendly alternatives. Although viable alternatives exist for medium voltage (e.g. vacuum breakers), equally effective substitutes are not yet available for high voltage. Therefore, SF_6 will likely remain the preferred choice for GIS in the near future.

Since the performance of the gas depends on its density, GIS systems are filled

with a reserve of SF_6 (5–20% more than the minimum required), allowing leak detection before performance degradation occurs [34].

3.4.2 Construction and Components

GIS (Gas-Insulated Substations) systems are assembled from standardized modules, including:

- Circuit breakers
- Current transformers (CT) and voltage transformers (VT)
- Disconnectors and grounding switches
- Interconnection busbars
- Surge arresters
- Network connection points

The modular configuration allows adaptation of the system to the substation's single-line diagram, as shown in Figure 3.7.

The interconnection between modules is achieved through an integrated system of mechanical and electrical joints. Bolted flanges equipped with O-ring seals ensure system tightness. Internal conductors are connected via plug-in sliding contacts with extremely low resistance.

This modular configuration offers significant management advantages. In particular, the sealed compartments allow for quick identification of gas leaks and limit gas contamination in case of internal failure, confining issues to a single module.

The housing is generally made of aluminum due to its light weight and corrosion resistance. Steel can also be used, being more economical but requires anti-corrosion treatment (painting). Internal periodic maintenance is not required, making GIS a reliable solution for both indoor and outdoor installations, with a service life exceeding 50 years.

3.4.3 Single-Phase and Three-Phase GIS

For magnetic field calculation purposes, it is important to distinguish between single-phase (Figure 3.8) and three-phase (Figure 3.9) GIS configurations. In the single-phase arrangement, a single enclosure is used for all three phases. This is feasible for $V_n < 170\,\text{kV}$, as higher voltages require larger dimensions, making the three-phase configuration impractical. The single-phase configuration can also be used for lower voltages (e.g. 132 kV, 150 kV)

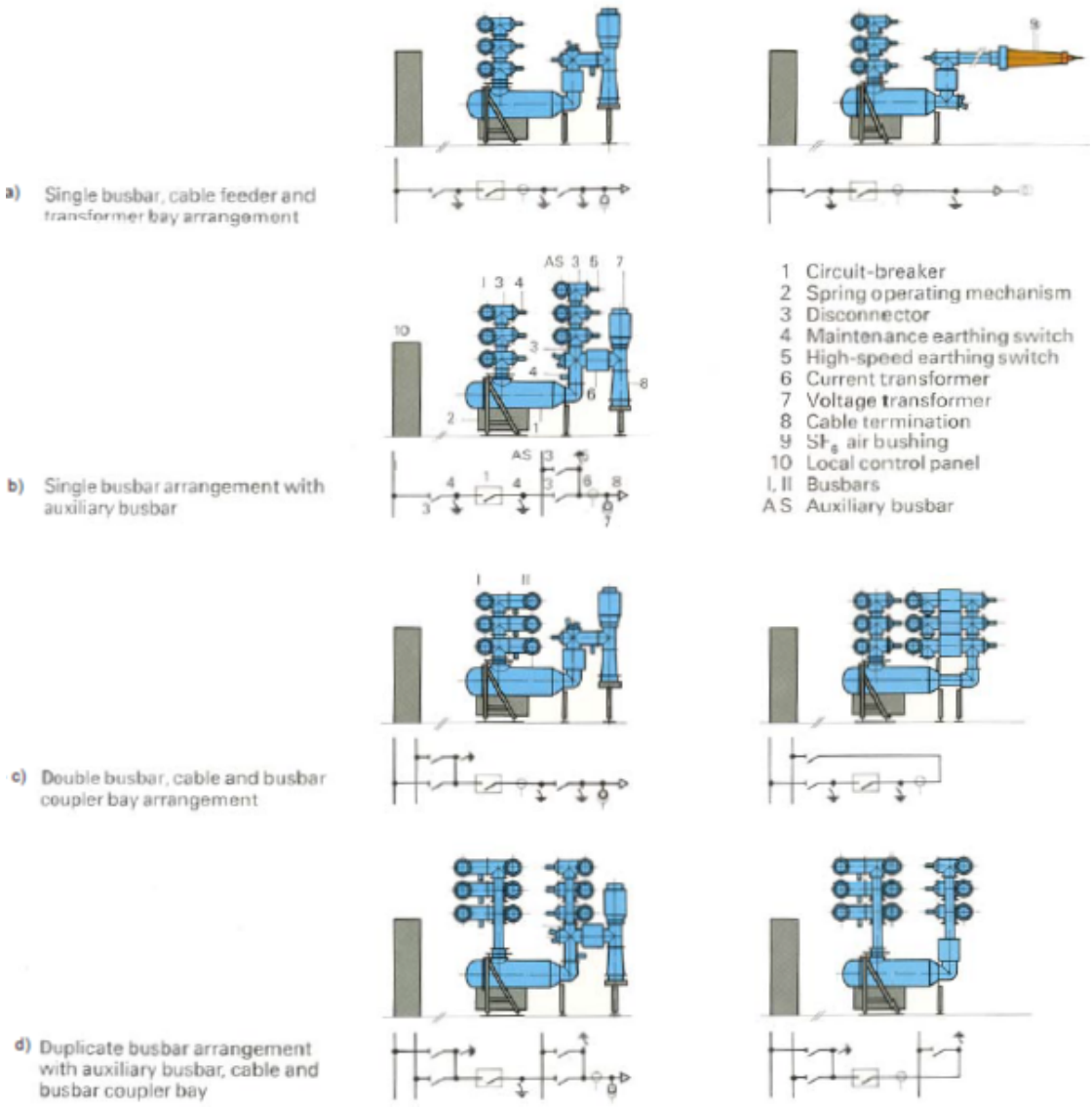

Figure 3.7: Examples of GIS configurations [36].

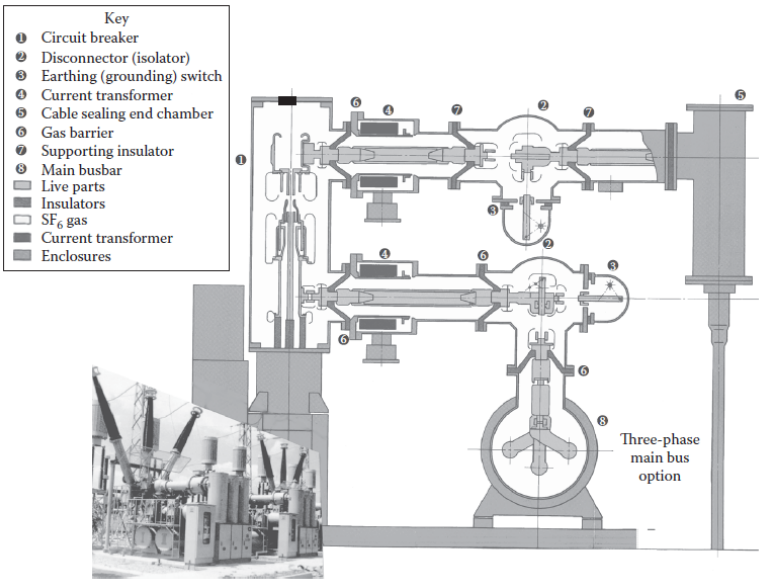

Figure 3.8: Single-phase GIS enclosure [34].

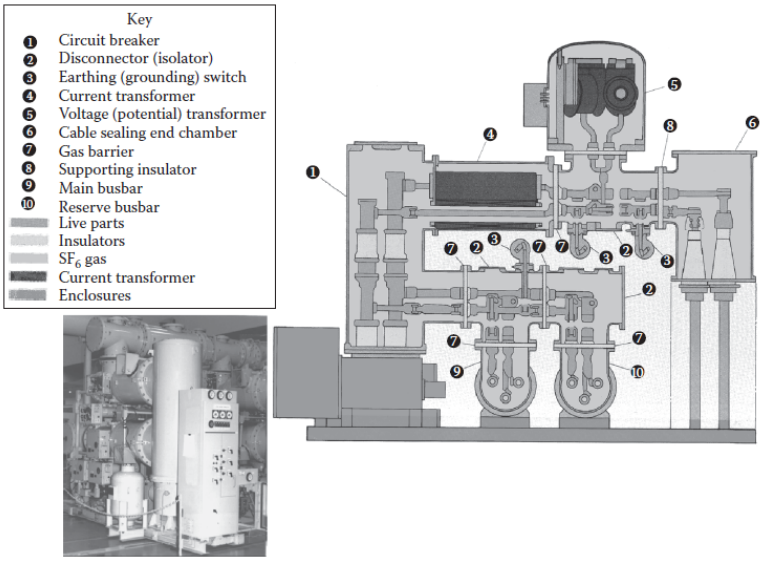

Figure 3.9: Three-phase GIS enclosure [34].

3.4.4 Grounding

The electrical continuity of the metallic sections of the GIS enclosure is ensured by external jumpers bolted to the flanges or dedicated grounding plates. Alternatively, self-supporting flange joints can be used, which are designed to autonomously guarantee electrical continuity.

Early GIS designs commonly used a single-point grounding system to prevent stray currents. The current standard requires multi-grounding, despite the losses caused by induced currents. This configuration provides multiple paths for fault currents to reach the grounding grid, helping to keep step and touch voltages within safety limits, and thus ensuring operator protection [37]. Figure 3.10 shows the two types of grounding.

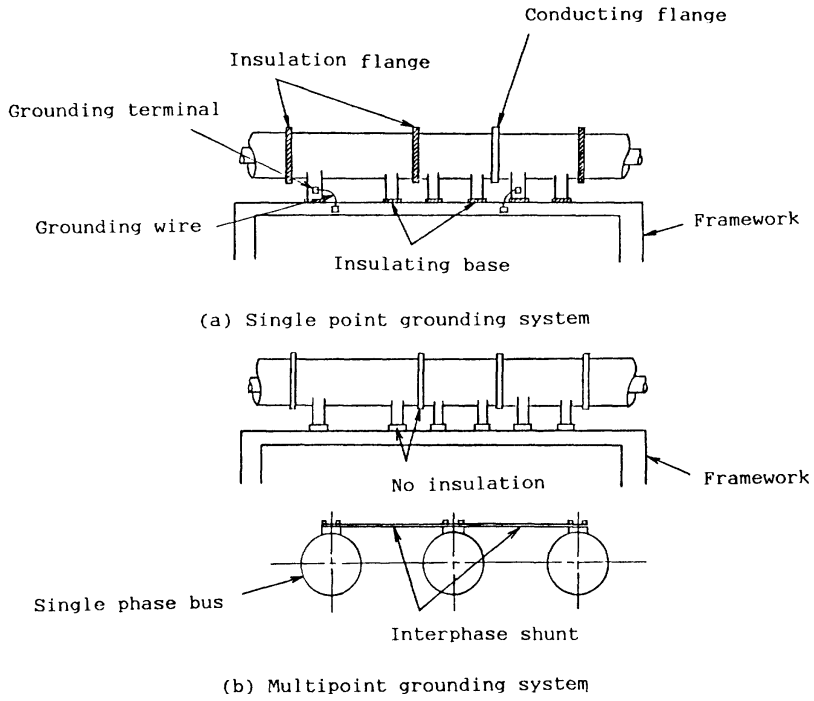

Figure 3.10: GIS grounding system [37].

3.4.5 Qualitative Analysis of Magnetic Field

In three-phase GIS, conductors are closely spaced and the mutual cancellation effect of magnetic fields between phases is very pronounced. Under these conditions, the enclosure acts as an effective shield for the magnetic field, which becomes negligible outside. Indeed, applying Ampère's law (1.4), we observe that the net current linked to the enclosure is zero.

In the case of single-phase GIS with multi-grounding systems, the electrical connection between the three enclosures at the installation ends allows the circulation of induced currents. According to Lenz's law, these generate a magnetic field opposing that of the main conductor, thereby reducing the overall external magnetic field. Figure 3.11 shows the magnetic field emitted by a 500 kV - 8 kA GIS, compared with theoretical values calculated for a single-ground configuration.

In the second case, the phases - being contained in separate and non-interacting enclosures - generate unbalanced magnetic fields. The enclosure therefore experiences a non-zero linked current, and Ampère's law predicts a net circulation of the field, resulting in a significantly higher external magnetic field.

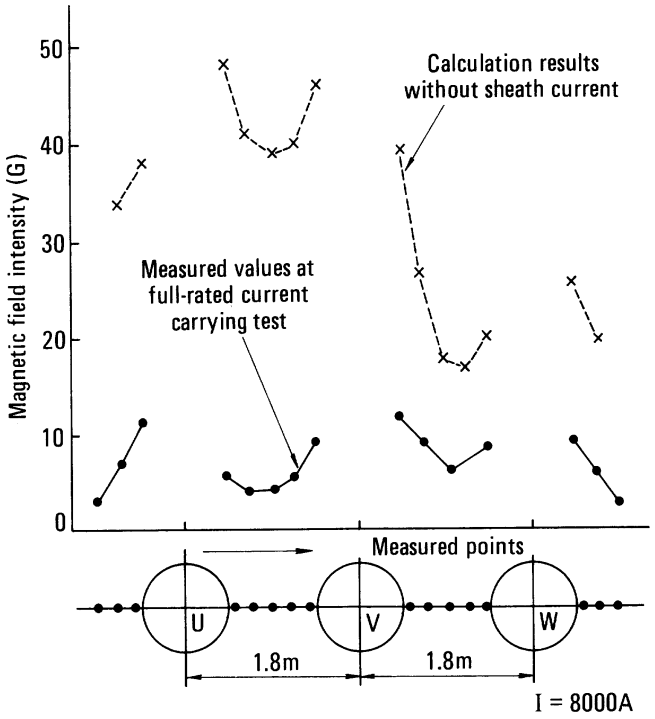

Figure 3.11: Magnetic field produced by 8kA GIS [37].

1 G (Gauss) = 10^{-4} T (Tesla).

3.4.6 Qualitative Analysis of Electric Field

GIS enclosures are metallic, therefore through the Faraday cage effect, the static electric field generated inside the system cannot propagate outward. Furthermore, the enclosures are grounded, ensuring zero residual charge outside and thus canceling the electric field outside the equipment, making it negligible. This principle is effective for both three-phase and single-phase GIS.

From an electrostatic perspective, the metallic enclosure acts as a perfect shield, maintaining constant external potential and preventing any electric field effects on surrounding structures. Moreover, during normal operating conditions, capacitive stresses between phases and between phases and ground are completely contained within the enclosure. The maximum electric field is localized near internal insulators but is effectively confined by the system [38].

3.5 Air-Insulated Substations (AIS)

Air-insulated substations represent a well-established and widely used solution for high-voltage electrical substations. In this configuration, insulation between active parts is provided by atmospheric air, which acts as a natural dielectric medium. The construction simplicity helps contain production costs, making AIS an economically advantageous choice in many operational scenarios.

However, insulation effectiveness is strongly influenced by environmental conditions: humidity, salt (especially near coastal areas), dust and corrosive agents can deposit on insulating surfaces, compromising insulation distances and increasing the risk of partial discharges or electrical arcs. This necessitates preventive measures and regular maintenance to ensure plant reliability.

3.5.1 Qualitative Analysis of Electric and Magnetic Fields

AIS represents a technically reliable and cost-effective solution, but involves greater exposure to electric and magnetic fields and requires larger physical spaces.

Regarding the electric field, AIS lack electrostatic shielding typical of metallic GIS enclosures. Consequently, the static electric field generated between phases and between phases and ground propagates freely in the surrounding space. The larger insulation distances required to ensure dielectric withstand in air lead to a greater plant footprint and higher exposure of active components (bare conductors, insulators and busbars). This results in a more extensive and more intense external electric field.

Concerning the magnetic field in AIS, phase conductors are typically spaced apart to meet air insulation requirements. This configuration results in less effective magnetic field cancellation compared to GIS, where conductors are closely spaced.

Chapter 4

Definition of the theoretical models

This chapter defines the theoretical models used in the computational code developed for this thesis work. The adopted models favor analytical approaches over finite element methods to reduce computational costs. A simplified analytical model will also be presented, which can be easily used with "pen and paper", thus serving as a powerful tool for technical support.

4.1 Electric Field Model

This section describes the numerical model adopted for calculating the electric field generated by a system of n conductors within an electrical substation. The approach is based on the method of virtual images, which accounts for the effect of the ground plane in evaluating the induced charges q on the conductors and, subsequently, in calculating the electric field. The ground is assumed to be ideal (homogeneous and perfectly conductive).

The potential V_i on the i-th conductor is expressed as:

$$V_i = \sum_{j=1}^{n} P_{ij} q_j \tag{4.1}$$

where P_{ij} are the potential coefficients, which include both the direct and the image conductors' contributions. The coefficient P_{ij} represents the potential on conductor i produced by a unit charge placed on conductor j and depends exclusively on the system's geometry.

Each real segment, bounded by the endpoints $P_1 = (x_1, y_1, z_1)$ and $P_2 = (x_2, y_2, z_2)$, generates an image segment between points $P_1' = (x_1, y_1, -z_1)$ and

$P'_2 = (x_2, y_2, -z_2)$, relative to the ground plane ($z = 0$). The coefficient P_{ij} is calculated according to the following expression [39]:

$$P_{ij} = \frac{1}{4\pi\varepsilon_0 d_j} \ln\left(\frac{(L_1 + L_2 + d_j)(L'_1 + L'_2 - d_j)}{(L_1 + L_2 - d_j)(L'_1 + L'_2 + d_j)}\right) \tag{4.2}$$

where:

- d_j is the length of segment j,
- L_1 and L_2 are the distances from the centroid of segment i to the endpoints of segment j,
- L'_1 and L'_2 are the corresponding distances relative to the image segment j'.

For the diagonal terms P_{ii} ($i = j$), the distances must be calculated with respect to the conductor's surface rather than its centroid. Figure 4.1 illustrates these quantities for clarity.

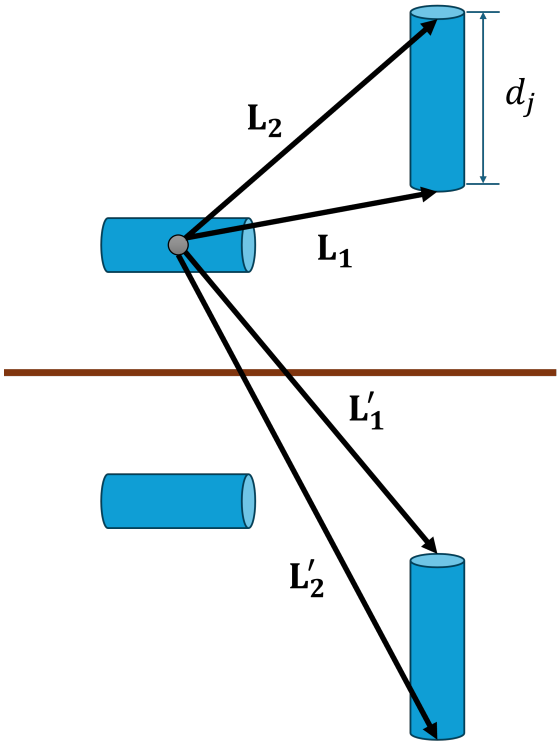

Figure 4.1: Geometric model for calculating potential coefficients.

Once all coefficients P_{ij} are determined, knowing the conductors' potentials, the linear system 4.1 is solved to obtain the charge q_j on each conductor. which is

assumed equally distributed. When the system is supplied by a sinusoidal voltage $\underline{V}$, the charges $\underline{q}_j$ will also exhibit a sinusoidal time-domain behavior.

With the charges $\underline{q}$ calculated, the complex electric field $\underline{\mathbf{E}}$ at a point Q is obtained by summing the contributions from all real segments and their corresponding images. The x-component of the field is expressed as:

$$\underline{E}_x = \sum_{i=1}^{n} \frac{\underline{q}_i}{4\pi\varepsilon_0 d_i} \left[\left(\frac{x_Q - x_1^i}{L_{1,i}} + \frac{x_Q - x_2^i}{L_{2,i}} \right) G_1^i - \left(\frac{x_Q - x_1^i}{L'_{1,i}} + \frac{x_Q - x_2^i}{L'_{2,i}} \right) G_2^i \right] \quad (4.3)$$

where:

$$G_1^i = \frac{1}{L_{1,i} + L_{2,i} - d_i} - \frac{1}{L_{1,i} + L_{2,i} + d_i} \quad (4.4)$$

$$G_2^i = \frac{1}{L'_{1,i} + L'_{2,i} - d_i} - \frac{1}{L'_{1,i} + L'_{2,i} + d_i} \quad (4.5)$$

The terms G_1^i and G_2^i derive from the integration of the linear charge density, assumed constant, along each segment [39]. Specifically, G_1^i represents the contribution from the real segment, while G_2^i accounts for the image segment, ensuring compliance with the boundary conditions imposed by the ground plane.

The quantities:

- $L_{1,i}$ and $L_{2,i}$ are the distances from point Q to the endpoints of real segment i,
- $L'_{1,i}$ and $L'_{2,i}$ are the corresponding distances for image segment i',
- d_i is the length of segment i.

Figure 4.2 illustrates the geometric quantities required for calculating the electric field $\underline{\mathbf{E}}$ at a generic observation point. The y and z components of the electric field are calculated similarly [39]:

$$\underline{E}_y = \sum_{i=1}^{n} \frac{\underline{q}_i}{4\pi\varepsilon_0 d_i} \left[\left(\frac{y_Q - y_1^i}{L_{1,i}} + \frac{y_Q - y_2^i}{L_{2,i}} \right) G_1^i - \left(\frac{y_Q - y_1^i}{L'_{1,i}} + \frac{y_Q - y_2^i}{L'_{2,i}} \right) G_2^i \right] \quad (4.6)$$

$$\underline{E}_z = \sum_{i=1}^{n} \frac{\underline{q}_i}{4\pi\varepsilon_0 d_i} \left[\left(\frac{z_Q - z_1^i}{L_{1,i}} + \frac{z_Q - z_2^i}{L_{2,i}} \right) G_1^i - \left(\frac{z_Q + z_1^i}{L'_{1,i}} + \frac{z_Q + z_2^i}{L'_{2,i}} \right) G_2^i \right] \quad (4.7)$$

For the purpose of determining the right-of-way, the maximum value of the electric field in the time domain is of interest, which corresponds to the magnitude of the field phasor vector:

$$E_{\max}(Q) = |\underline{\mathbf{E}}(Q)|. \quad (4.8)$$

This model assumes that only air with constant permittivity (ε_0) exists between the conductors and the observation point.

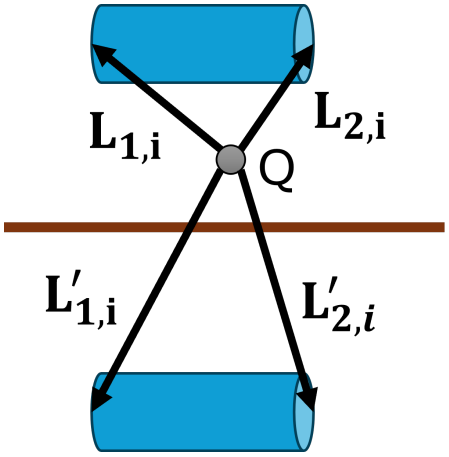

Figure 4.2: Geometric model for electric field calculation.

4.1.1 Model Application in Substations

In the context of electric field assessment, it is necessary to distinguish between AIS (Air Insulated Substation) and GIS (Gas Insulated Substation) configurations, as their contribution to external emissions differs substantially.

For GIS substations, the conductors are completely enclosed within a grounded metal casing that acts as an effective electrostatic shield. Regardless of the internal conductor configuration (single-phase or multi-phase), the metal enclosure maintains a uniform potential and prevents electric field propagation to the exterior. Consequently, GIS sections can be excluded from the electric field calculation domain, as their influence on the surrounding space is negligible under quasi-static conditions.

Conversely, in AIS substations, conductors are exposed to the environment and are therefore the primary sources of external electric field emissions. In such configurations, the charge distribution and resulting electric field depend directly on conductor geometry, their height above ground and the distance from the observation point.

The model described in the previous section, based on the method of images, is thus applied exclusively to AIS conductors where shielding effects are absent and charge modeling is essential for accurate field estimation. This assumption allows significant problem simplification without compromising accuracy, as the containment effectiveness of GIS metal enclosures is complete steady state.

4.2 Induction Magnetic Field Model

The magnetic field generated by a finite-length straight conductor carrying current can be determined through the analytical expression derived from the Biot-Savart law.

Consider a straight conductor carrying sinusoidal alternating current, represented in complex phasor form as $\underline{I} = Ie^{j\varphi}$, with endpoints at $P_1 = (x_1, y_1, z_1)$ and $P_2 = (x_2, y_2, z_2)$. The magnetic field phasor $\underline{\mathbf{B}}$ at a generic point $Q = (x_Q, y_Q, z_Q)$, as shown in Figure 4.3, is given by:

$$\underline{\mathbf{B}}(Q) = \frac{\mu_0 \underline{I}}{4\pi} \int_{P_1}^{P_2} \frac{\mathbf{dl} \times \mathbf{r}}{|\mathbf{r}|^3} \tag{4.9}$$

where:

- **dl** is the infinitesimal length element oriented along the conductor;
- **r** is the distance vector from element **dl** to observation point Q.

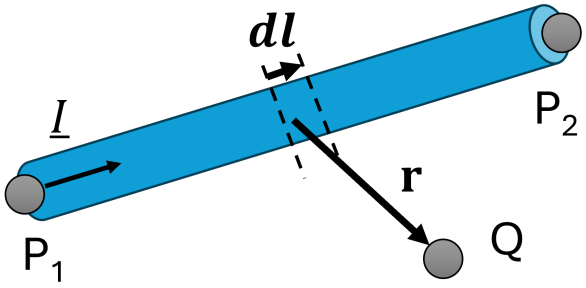

Figure 4.3: Representation of the model for magnetic field calculation.

The use of phasor notation for a vector quantity like the magnetic field allows us to construct the temporal behavior of the field and sum field values produced by three-phase systems, even when time-shifted. The integral in 4.9 admits a closed-form analytical solution [40], with magnetic field components expressed as:

$$\underline{B}_x(Q) = \frac{\mu_0 \underline{I}}{4\pi} k_x \mathcal{F}(a, b, c) \tag{4.10}$$

$$\underline{B}_y(Q) = \frac{\mu_0 \underline{I}}{4\pi} k_y \mathcal{F}(a, b, c) \tag{4.11}$$

$$\underline{B}_z(Q) = \frac{\mu_0 \underline{I}}{4\pi} k_z \mathcal{F}(a, b, c) \tag{4.12}$$

where coefficients k_x, k_y, and k_z are defined as:

$$k_x = y_1(z_2 - z_Q) + y_2(z_Q - z_1) + y_Q(z_1 - z_2) \tag{4.13}$$
$$k_y = -\left[x_1(z_2 - z_Q) + x_2(z_Q - z_1) + x_Q(z_1 - z_2)\right] \tag{4.14}$$
$$k_z = x_1(y_2 - y_Q) + x_2(y_Q - y_1) + x_Q(y_1 - y_2) \tag{4.15}$$

The common factor $\mathcal{F}(a, b, c)$ is defined as:

$$\mathcal{F}(a, b, c) = \frac{2}{4ac - b^2}\left(\frac{2a - b}{\sqrt{a - b + c}} + \frac{b}{\sqrt{c}}\right) \tag{4.16}$$

with geometric parameters:

$$a = (x_1 - x_2)^2 + (y_1 - y_2)^2 + (z_1 - z_2)^2 \tag{4.17}$$
$$b = 2\left[(x_1 - x_2)(x_1 - x_Q) + (y_1 - y_2)(y_1 - y_Q) + (z_1 - z_2)(z_1 - z_Q)\right] \tag{4.18}$$
$$c = (x_1 - x_Q)^2 + (y_1 - y_Q)^2 + (z_1 - z_Q)^2 \tag{4.19}$$

This approach can be extended to multi-conductor configurations through superposition. The total magnetic field at point Q is obtained as the vector sum of contributions $\underline{\mathbf{B}}_k(Q)$ from each conductor segment k:

$$\underline{\mathbf{B}}(Q) = \sum_{k=1}^{n} \underline{\mathbf{B}}_k(Q) \tag{4.20}$$

Once the total magnetic field is determined in phasor form, for right-of-way assessment it is useful to calculate the maximum time-domain field value, corresponding to the phasor vector magnitude:

$$B_{\max}(Q) = \left|\underline{\mathbf{B}}(Q)\right|. \tag{4.21}$$

This model assumes a homogeneous and non-magnetic environment with constant permeability μ_0 (air).

4.2.1 Model Application in Substations

In this analysis, conductors in AIS and GIS substations are approximated as straight filamentary segments, an assumption valid when observation distances are much greater than conductor radius.

For three-phase GIS configurations, the metal shielding contains all phases at very close distances. Consequently, the integral in 4.9 assumes similar values for each phase:

$$\underline{\mathbf{B}}(Q) = \sum_{k=1}^{3} \left(\frac{\mu_0 \, \underline{I}_k}{4\pi} \int_{P_{1_k}}^{P_{2_k}} \frac{\mathbf{dl}_k \times \mathbf{r}_k}{|\mathbf{r}_k|^3} \right) \approx \frac{\mu_0}{4\pi} \int_{P_1}^{P_2} \frac{\mathbf{dl} \times \mathbf{r}}{|\mathbf{r}|^3} \sum_{k=1}^{3} \underline{I}_k \tag{4.22}$$

The resulting external magnetic field is negligible because the system is balanced three-phase and the current phasor sum is zero ($\sum \underline{I}_k = 0$ A).

For single-phase GIS configurations, the model adequately describes the generated magnetic field with single-point grounding. With multi-point grounding, the model remains applicable if induced currents in metal enclosures are known, which can be represented as straight filamentary conductors coaxial to the enclosure. For conservative assessment, induced current effects may be neglected, as this overestimates field levels and thus provides safer evaluations. Magnetic emissions are reduced compared to AIS substations, thanks to gas insulation allowing smaller phase separations that promote more effective field cancellation.

4.3 Simplified Model

The assessment of magnetic field emissions in HV substations can be effectively carried out using a far-field approximation model. This approach allows for a simplified analysis. In this section, the model equations are derived.

Consider a system composed of N infinitely long, straight, and parallel conductors aligned along the z-axis, each carrying a complex current $\underline{I}_k$. The magnetic field is evaluated on the xy-plane, with each conductor k located at point $\mathbf{r}_k = (x_k,\ y_k)$, and the observation point at $\mathbf{r} = (x,\ y)$, as shown in Figure 4.4. The complex magnetic field $\underline{\mathbf{B}}$ generated by the system is described by the Biot–Savart law:

$$\underline{\mathbf{B}}(\mathbf{r}) = \frac{\mu_0}{2\pi} \sum_{k=1}^{N} \underline{I}_k \frac{\mathbf{a}_z \times (\mathbf{r} - \mathbf{r}_k)}{|\mathbf{r} - \mathbf{r}_k|^2} \tag{4.23}$$

where $\mathbf{a}_z$ is the unit vector along the z-axis.

By translating the reference system to the centroid of the conductor configuration, defined as:

$$\mathbf{r}_0 = \frac{1}{N} \sum_{k=1}^{N} \mathbf{r}_k \tag{4.24}$$

we introduce the following vectors relative to the centroid:

- $\mathbf{R} = \mathbf{r} - \mathbf{r}_0$: position of the observation point relative to the centroid,
- $\mathbf{d}_k = \mathbf{r}_k - \mathbf{r}_0$: position of conductor k relative to the centroid.

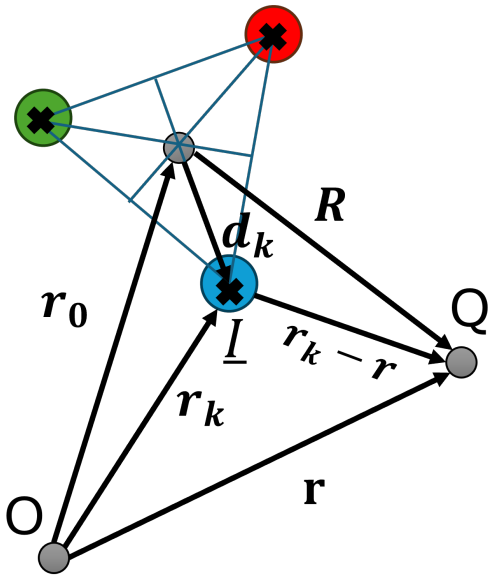

Figure 4.4: Geometric representation of the simplified model

Since $\mathbf{r} - \mathbf{r}_k = \mathbf{R} - \mathbf{d}_k$, the magnetic field expression becomes:

$$\underline{\mathbf{B}}(\mathbf{R}) = \frac{\mu_0}{2\pi} \sum_{k=1}^{N} \underline{I}_k \mathbf{a}_z \times \frac{(\mathbf{R} - \mathbf{d}_k)}{|\mathbf{R} - \mathbf{d}_k|^2} \tag{4.25}$$

Assuming the observation point is sufficiently far from the conductor system ($R \gg d_k$), a first-order series expansion of the denominator can be performed to simplify the field expression. In particular, we observe that:

$$|\mathbf{R}-\mathbf{d}_k|^2 = (\mathbf{R}-\mathbf{d}_k)\cdot(\mathbf{R}-\mathbf{d}_k) = R^2 - 2\mathbf{R}\cdot\mathbf{d}_k + d_k^2 = R^2\left(1 - 2(\mathbf{a}_R \cdot \mathbf{a}_{d_k})\frac{d_k}{R} - \frac{d_k^2}{R^2}\right) \tag{4.26}$$

The Taylor series expansion of $\frac{1}{1-x} = \sum x^n$ with $x = 2(\mathbf{a}_R \cdot \mathbf{a}_{d_k})\frac{d_k}{R} - \frac{d_k^2}{R^2}$ gives, up to first order:

$$\frac{1}{|\mathbf{R} - \mathbf{d}_k|^2} = \frac{1}{R^2}\left(1 + 2(\mathbf{a}_R \cdot \mathbf{a}_{d_k})\frac{d_k}{R} + o(\frac{d_k}{R})\right) \tag{4.27}$$

Expanding the numerator $\mathbf{R} - \mathbf{d}_k = R(\mathbf{a}_R - \mathbf{a}_{d_k}\frac{d_k}{R})$ and dividing by the denominator, we get:

$$\frac{\mathbf{R} - \mathbf{d}_k}{|\mathbf{R} - \mathbf{d}_k|^2} = \frac{1}{R}(\mathbf{a}_R + (2\mathbf{a}_R(\mathbf{a}_R \cdot \mathbf{a}_{d_k}) - \mathbf{a}_{d_k})\frac{d_k}{R} + o(\frac{d_k}{R})) \tag{4.28}$$

The resulting magnetic field can then be expressed as a sum of terms with different decay rates as a function of distance, allowing for a simplified evaluation of far-field emissions. The expression for $\underline{\mathbf{B}}(\mathbf{R})$ in (4.25) can be approximated using the first-order Taylor expansion:

$$\underline{\mathbf{B}}(\mathbf{R}) \approx \underline{\mathbf{B}}_0(\mathbf{R}) + \underline{\mathbf{B}}_1(\mathbf{R}) \tag{4.29}$$

Zero-Order Term

$$\underline{\mathbf{B}}_0(\mathbf{R}) = \frac{\mu_0}{2\pi R}(\mathbf{a}_z \times \mathbf{a}_R)\sum_{k=1}^{N}\underline{I}_k \tag{4.30}$$

This term decays as $1/R$ and vanishes for a balanced system ($\sum_{k=1}^{N}\underline{I}_k = 0$). This condition holds in HV substations, as they operate under balanced three-phase conditions.

First-Order Term

$$\mathbf{B}_1(\mathbf{R}) = \frac{\mu_0}{2\pi R^2}\left[2(\mathbf{a}_R \cdot \mathbf{M}_1)(\mathbf{a}_z \times \mathbf{R}) - \mathbf{a}_z \times \mathbf{M}_1\right] \tag{4.31}$$

where the current dipole moment $\mathbf{M}_1$ is defined as:

$$\mathbf{M}_1 = \sum_{k=1}^{N}\underline{I}_k\mathbf{d}_k \tag{4.32}$$

The second-order term vanishes if the dipole moment is zero, which can be achieved using the split-phase technique. However, this is not typically implemented in HV substations, making this term the most significant. As shown, the magnetic field decays with the square of the distance.

4.3.1 Model Application in Substations

In high-voltage (HV) substations, conductors are generally arranged in a planar configuration, with phase spacing d, as shown in Figure 4.5. The centroid of the system coincides with the central conductor and, since the system operates under balanced conditions ($|\underline{I}_k| = I$), the magnitude of the magnetic field in the far-field region is dominated by the first-order term (4.31). For this specific configuration, the expression simplifies to:

$$B(R) \approx \frac{\mu_0 \sqrt{3}}{2\pi} \frac{Id}{R^2} \tag{4.33}$$

As previously discussed, this expression is valid only in the far-field region, that is, when the observation point is significantly farther than the geometric dimensions of the conductor system. This simplified model proves particularly useful for assessing compliance with exposure limits to low-intensity magnetic fields, such as the threshold values of $3\,\mu$T and $10\,\mu$T adopted by Italian regulations.

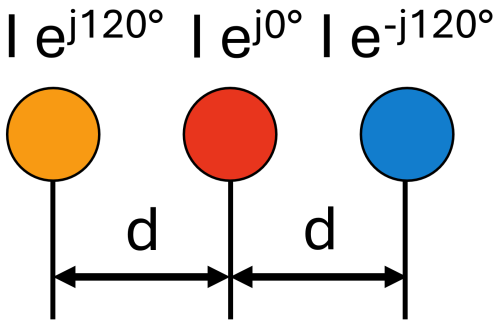

Figure 4.5: Planar configuration of a three-phase system

By solving for the distance R corresponding to the threshold levels defined by the DPCM of July 8, 2003 [1], the following expressions are obtained:

$$R_{3\mu T} \approx 0.34\sqrt{Id} \tag{4.34}$$

$$R_{10\mu T} \approx 0.19\sqrt{Id} \tag{4.35}$$

$$R_{100\mu T} \approx 0.059\sqrt{Id} \tag{4.36}$$

These formulas allow for a quick estimation of clearance distances (Figure 4.6) associated with different magnetic field intensity levels. The next section will analyze the validity of the simplified model, highlighting, for instance, that the expression for the $100\,\mu$T level (4.36) is not practically applicable, as the resulting

values of R do not meet the far-field condition ($R \gg d$), which is necessary for the accuracy of the approximation.

In the ideal case of an infinitely long conductor, the region where $B > 3\,\mu\text{T}$ takes the form of a cylinder with radius $R_{3\mu T}$ and axis aligned with the system centroid.

However, it is important to emphasize that the model assumes infinitely long conductors. In real substations, the finite length of conductors introduces edge effects that reduce the magnetic field near the ends. As a result, the far-field model tends to overestimate the field, providing a safety margin.

In the more realistic case of conductors with finite length L, the region where the magnetic field exceeds the regulatory threshold becomes a solid of revolution: a cylinder of length L and radius $R_{3\mu T}$, centered on the system centroid (the central conductor in the planar configuration) and closed at both ends by hemispheres of the same radius. The intersection of this volume with a given plane determines the $B = 3\,\mu\text{T}$ isoline of the magnetic field on that plane.

In practical applications, a useful and conservative simplification consists in neglecting the elevation of the observation point, i.e. considering the intersection of the revolution solid with the plane containing the conductors. In this way, the clearance zone is approximated by a two-dimensional shape consisting of a rectangle with length equal to that of the conductor and height $2R_{3\mu T}$, completed at both ends by two semicircles of radius $R_{3\mu T}$. This approximation, although conservative, greatly simplifies the estimation of areas subject to magnetic fields exceeding the regulatory threshold, proving particularly useful during the design or environmental assessment phases. This allows the clearance zone to be directly represented on the substation layout, based solely on the known values of nominal current and phase spacing, by applying the simple formula (4.34).

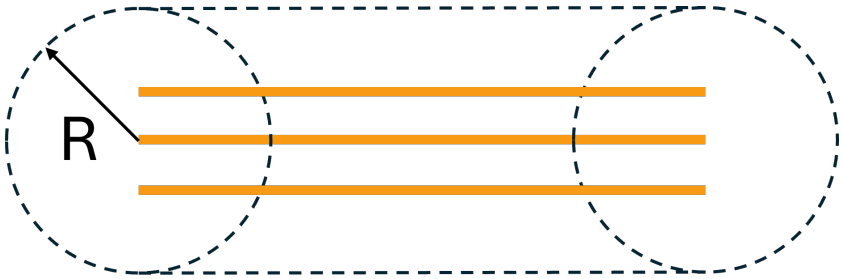

Figure 4.6: Clearance zone in the far-field approximation for a three-phase planar system

4.3.2 Considerations on the Validity of the Simplified Model

As previously discussed, the simplified model is valid only in the far-field region, i.e. when the observation point is sufficiently distant compared to the geometric dimensions of the system. This section provides a quantitative estimate of the validity domain by evaluating the error associated with the adopted approximation.

The series expansion considered is given by equation 4.28. To evaluate the maximum error, the configuration in which vectors $\mathbf{R}$ and $\mathbf{d_k}$ are parallel is considered, as this condition maximizes the truncation error of the series. In this case, a scalar treatment—which is simpler—can be adopted:

$$\frac{\mathbf{R}-\mathbf{d}_k}{|\mathbf{R}-\mathbf{d}_k|^2} = \frac{R-d_k}{(R-d_k)^2} = \frac{1}{R}\frac{1}{1-\frac{d_k}{R}} \tag{4.37}$$

Setting $x = \frac{d_k}{R}$, and approximating the expansion $\frac{1}{1-x} = \sum x^n$ to first order, a relative error is introduced:

$$\varepsilon_r = \frac{\frac{1}{1-x} - (1+x)}{\frac{1}{1-x}} = x^2 \tag{4.38}$$

The error is calculated under the assumption of infinitely long conductors. Imposing a maximum tolerable error of 5% ($\varepsilon_\mathrm{r} < 0.05$), the following condition for the validity of the approximation is obtained:

$$R^2 > 20d^2 \tag{4.39}$$

This inequality defines the far-field region for the simplified model. Using the expression for the simplified magnetic field in a planar configuration (4.33) together with the validity condition (4.39), the minimum current I_min required to ensure the applicability of the model as a function of the phase spacing d is given by:

$$I_\mathrm{min} = \frac{2\pi}{\mu_0\sqrt{3}}\frac{R_\mathrm{min}^2 B}{d} = \frac{10^8\,B}{\sqrt{3}}\,d \tag{4.40}$$

Applying this relation to the regulatory threshold values defined by the DPCM of July 8, 2003 [1], conservative estimates of the minimum admissible currents are obtained:

$$I_{\mathrm{min},\ 3\ \mu\mathrm{T}} \approx 170\,d \tag{4.41}$$

$$I_{\mathrm{min},\ 10\ \mu\mathrm{T}} \approx 580\,d \tag{4.42}$$

$$I_{\mathrm{min},\ 100\ \mu\mathrm{T}} \approx 5\,800\,d \tag{4.43}$$

These results highlight that the adopted approximation is not suitable for evaluating high magnetic field levels (e.g., $100\,\mu$T), as the required currents to

meet the validity condition are unrealistically high for real-world installations. The formula may be cautiously used for 10 μT levels, limited to scenarios with small phase spacings and high currents. Conversely, for the 3 μT level—used as a design reference in current regulations—the model is generally valid in AIS substations, where typical phase spacing ranges from 2 to 5 meters [41].

It can thus be concluded that the simplified model is an effective tool for preliminary and design evaluations related to compliance with low-intensity magnetic field exposure limits, while it is inadequate for analyses concerning compliance with maximum exposure limits.

4.4 Transformer Modeling

In the analysis of electric and magnetic fields from electrical infrastructure, transformers represent complex field sources due to laminated magnetic cores and three-dimensional winding configurations.

This thesis adopts a simplified model neglecting direct winding contributions to external magnetic fields. This choice, supported by theoretical and practical considerations in literature [42] [43] [44], reduces computational complexity. HV substation transformers operate at high power and are exclusively oil-immersed types. In such transformers, windings are housed in metal tanks filled with insulating oil, serving dual purposes: dielectric insulation and effective electromagnetic shielding. This containment significantly reduces external magnetic field propagation. Thus, winding contributions to external fields can be neglected, while external electrical connections - particularly low-voltage ones - represent the primary field sources requiring modeling.

This approach proves particularly useful when assessing compliance with magnetic field exposure limits or designing mitigation solutions. Note that dry-type transformers in MV/LV secondary substations (not covered here) exhibit greater winding contributions due to absent metal shielding, requiring more detailed modeling.

Chapter 5

Numerical Code

The aim of this chapter is to provide a detailed explanation of the design and implementation of the numerical code developed in MATLAB for modeling the electric and magnetic fields generated by HV (High Voltage) and EHV (Extra High Voltage) electrical substations.

The developed code was conceived as a flexible and parametric tool, capable of adapting to different characteristics of EHV/HV substations, with particular reference to the axial arrangement of main components which is widely adopted.

In the proposed model, all conductors are represented as straight segments. As analyzed in the previous chapter, this representation is valid even for transformers since the dominant emissive component is associated with connection conductors.

Input data acquisition, both geometric and electrical, occurs through a graphical user interface (GUI). The data is organized within a structured matrix, where each row represents a conductor segment and lists its physical and electrical properties. Subsequently, the code processes the model and returns, as output, the spatial distribution of electric and magnetic fields over a defined domain.

Each conductor is described by the following terms:

- **Geometric parameters**: $P_1 = (x_1, y_1, z_1)$ (segment origin), $P_2 = (x_2, y_2, z_2)$ (segment end) and cross-sectional radius R;

- **Electrical parameters**: Voltage $\underline{V}$, current $\underline{I}$ and phase (1, 2 or 3).

By convention, the current is considered positive when flowing from P_1 to P_2. Although phase information plays no role in field calculations, it is a useful parameter for graphical representation of the substation, for verification and debugging activities.

5.1 Input Parameters

For proper modeling of the electrical substation, it is necessary to acquire from the user both geometric and electrical data of the plant to be analyzed, including: substation topology, voltage and current values, physical conductor paths.

To this end, a graphical user interface (GUI) was implemented in MATLAB, available in both English and Italian. Figure 5.1 shows an example.

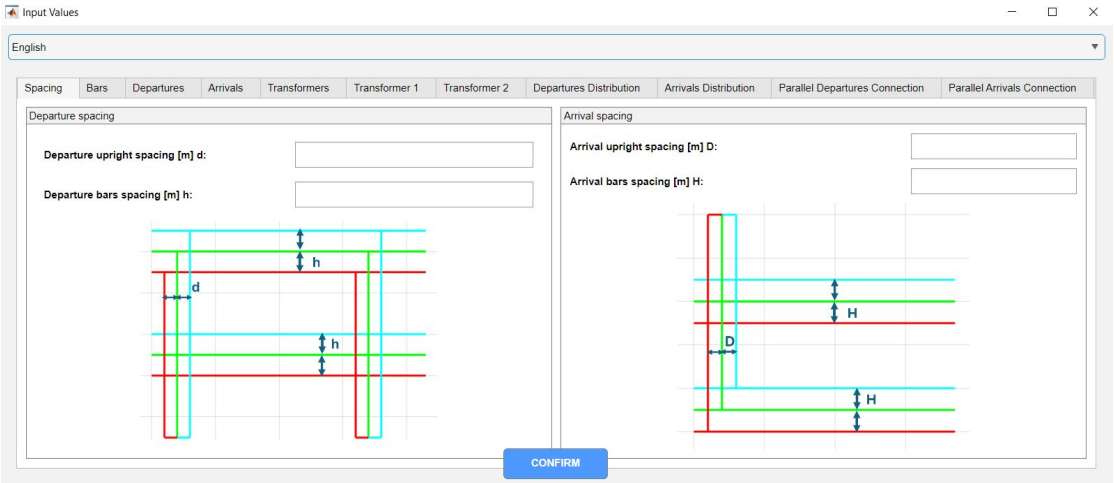

Figure 5.1: Graphical interface for entering substation parameters

The interface is organized into multiple thematic sections, complemented by illustrative images to guide the user, and covers three main categories: substation busbars, lines (incoming and outgoing), and transformers. For each category, the user must specify the following parameters:

- number of elements (e.g. *2 transformers, 1 incoming line, 4 outgoing lines*),
- rated current,
- conductor cross-section (assumed circular),
- spatial position of elements in Cartesian coordinates,
- phase spacing,
- substation configuration (e.g. *double busbar, single busbar, sectionalized busbar*),
- operational configuration (*line-busbar and transformer-busbar association during operation*).

The GUI also includes an input validation system. If the user enters an invalid value, a descriptive error message is generated, as shown in figure 5.2.

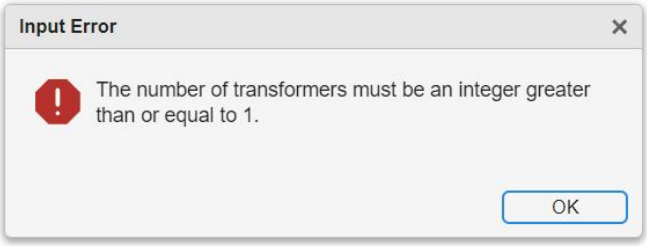

Figure 5.2: Example of error message during data entry

5.1.1 Transformers

The modeling of transformers in the developed code requires the definition of essential parameters, both electrical (nameplate data) and geometric (physical connections to conductors). This information is summarized in table 5.1, and users are shown figure 5.3 to clarify the required distances. In the case of a double busbar configuration, it is necessary to specify each transformer's association with its respective busbar (e.g. Busbar 1 or Busbar 2) to correctly reconstruct the system topology. The nominal voltage values defined uniformly for all transformers (V_{1n} and V_{2n}) are extended to all connected conductors and are used to define the substation's electrical profile.

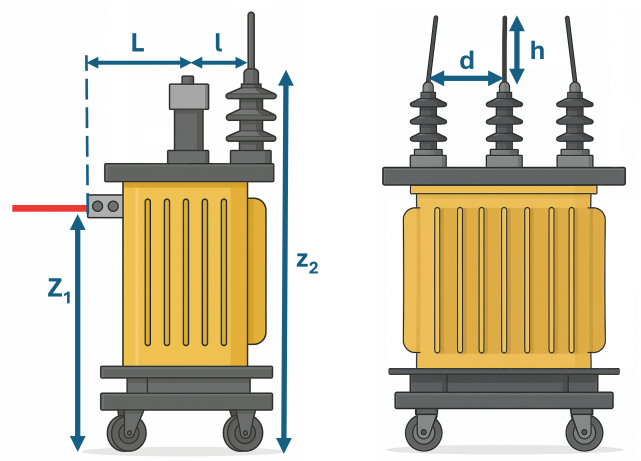

Figure 5.3: Transformer connection geometry

Table 5.1: Input parameters for transformers

Symbol	**Description**	**Unit**
N	Number of transformers	–
V_{1n}	Primary rated voltage	kV
V_{2n}	Secondary rated voltage	kV
g	Transformation group	–
x	Position	m
S_n	Rated power	MVA
$V_{cc\%}$	Nominal short-circuit voltage	%
d	LV terminal spacing	m
h	Oblique section length	m
l	Center-to-LV terminals distance	m
L	Center-to-HV terminals distance	m
z_1	LV terminals height	m
z_2	HV terminals height	m
S_1	HV connection conductor cross-section	mm^2
S_2	LV connection conductor cross-section	mm^2

5.1.2 Busbars

The modeling of substation busbars requires the specification of geometric parameters, with the main ones being:

- Cartesian coordinates position (y and z),
- Cross-section S (assumed circular),
- Busbar length L,
- Support height H,
- Phase spacing D.

In the GUI, this data is accompanied by an explanatory illustration (figure 5.4) that helps users understand the geometric meaning and enter the parameters correctly.

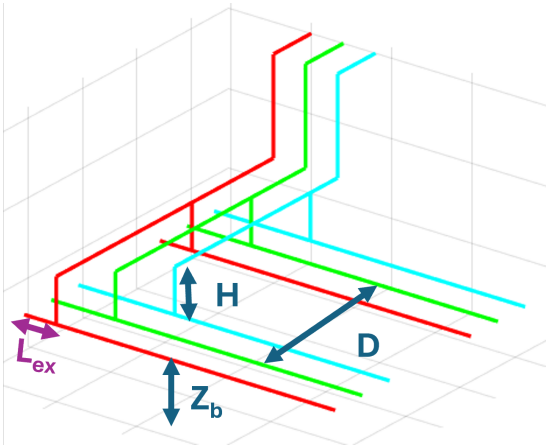

Figure 5.4: Geometric parameters of substation busbars

For double busbar configurations, additional parameters related to the bus coupler must be defined, used in configurations with main and transfer busbars or with single-breaker double busbars. Specifically, the spacing between the two busbars (D_c) and the coupler dimensions must be provided, as shown in figure 5.5.

Table 5.2 summarizes all parameters required for busbar definition, including additional data needed for more complex configurations. In sectionalized busbars, the coupler parameters must be provided for each segment.

5.1.3 Incoming/Outgoing Lines

The modeling of incoming (arrival) and outgoing (departure) lines requires the definition of the following fundamental parameters:

Table 5.2: Input parameters for substation busbars

Symbol	Description	Unit
N	Number of busbars	–
S	Busbar cross-section	mm^2
y	Busbar position	m
z	Busbar height	m
H	Support length	m
L	Busbar length	m
D	Phase spacing	m
Additional parameters for double busbar		
D_c	Center-to-center spacing	m
x_1	Coupler position	m
L_c	Coupler length	m
H_c	Coupler support length	m
S_c	Coupler cross-section	mm^2

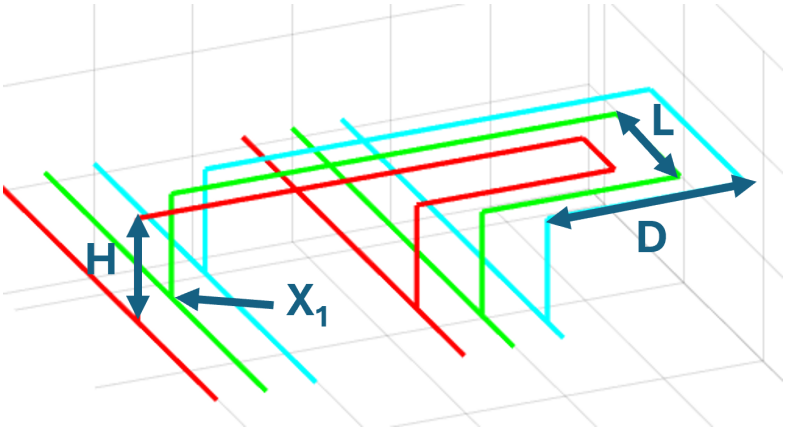

Figure 5.5: Geometric parameters of the bus coupler

- Spatial position (x, y, z) of the line arrival/departure point;
- Rated current I,
- Conductor cross-section S (assumed circular),
- Phase spacing D.

For substations with double busbar configuration, it is necessary to specify which busbar each line is connected to (e.g. Busbar 1 or 2), information critical for correct power flow simulation.

The complete parameters are summarized in Table 5.3.

Table 5.3: Input parameters for lines

Symbol	Description	Unit
N_p	Number of outgoing lines	–
N_a	Number of incoming lines	–
x, y, z	Line position	m
I	Line current	A
S	Line cross-section	mm^2
D	Phase spacing	m

5.2 Code Functions

After acquiring input data, the code proceeds with the parametric construction of the substation model. To optimize this process, dedicated functions were implemented to avoid code redundancy, minimize errors (e.g. copy-paste errors) and improve code readability and maintainability.

This was achieved by leveraging the typical symmetry of electrical substations where the EHV (Extra High Voltage) side mirrors the HV (High Voltage) side. This allowed using a single parametric function to model both sides. The design choice was to develop functions with reference to the HV side and call the same function for the EHV side by appropriately inverting parameters. This solution requires attention when calling functions for the EHV side as references and conventions must be properly adapted.

For example, the MATLAB code 5.1 shows the function call for generating incoming and outgoing lines. Code 5.2 shows the function header that documents through comments the necessary conventions for reusing the same function for incoming lines. The same logic was extended to other components: transformers, busbars and bus couplers.

```
% ========================================================
% GENERATION OF OUTGOING LINES (HV SIDE)
% ========================================================
outgoing_conductors=generateLines...
    (x_out, y_out, z_out,...                %line coordinates
y_bus1_out, dy_bus_out,...                  %Busbar position
z_bus_out, z_supp_out, ...                  %heights
d_line_out, d_bus, ...                      %phase spacing
section_out, ...
I_out, I_distr_out, ...                     %Current parameters
V_out);                                     %Rated voltage
% ========================================================
% GENERATION OF INCOMING LINES (EHV SIDE - HIGH VOLTAGE)
% ========================================================
%calculate final busbar position for incoming side
y_bus_N = y_bus1_in + dy_bus_in * (n_bus_in - 1);
%Adapt parameters for function call
incoming_conductors=generateLines ...
    (x_in, y_in, z_in, ...                  %incoming data
y_bus_N, -dy_bus_in, ...                    %Busbar position
z_bus_in, z_supp_in, ...                    %heights
d_line_in, d_bus, ...                       %phase spacing
section_in, ...
-I_in, I_distr_in(:,end:-1:1),...           %Current parameters
V_in);                                      %Rated voltage
```

MATLAB code 5.1: Function call for outgoing/incoming lines to the substation

```
function conductors=generateLines(...
...     % --- Geometric Input ---
x_line, y_line, z_line, ...          %line coordinates
y_bus1, delta_y_bus, ...             %nearest busbar and spacing
z_bus, z_support, ...                %heights
d_phase_line, d_phase_bus, ...       %phase spacing
section, ...
...     % --- Electrical Input ---
I_line, I_distribution, ...      %current and busbar distribution
V)                               %Rated voltage
    %-------------------------------------------------------------
    % CONDUCTOR GENERATION FOR OUTGOING LINES
    %
    % conventions for reuse with INCOMING LINES:
    % 1. Busbar coordinates:
    %    - y_bus1: for incoming, use busbar N
    %    - delta_y_bus: for incoming, invert sign
    %
    % 2. Current:
    %    - Sign: positive if flowing from busbar to line.
    %                For incoming, use -I_line
    %    - I_distribution: for incoming, reverse column order
    %                since we start from busbar N.
    %-------------------------------------------------------------
    ...     %Function body
end
```

MATLAB code 5.2: Function header for outgoing/incoming lines to the substation

5.3 Debugging

During code development, the adoption of debugging tools proved crucial to ensure model accuracy. This section describes the main implemented tools, useful both for verification during development and for potential future modifications.

5.3.1 3D Conductor Map

An essential debugging tool is the three-dimensional plot of conductors, which allows verifying the correct spatial arrangement of segments (P_1 and P_2), identifying errors in phase sequence (represented with different colors) and detecting misalignment between adjacent components (e.g. supports-busbars). Code 5.3 generates a 3D map highlighting start and end points with circular markers. Figure 5.6 shows the code output where errors can be easily observed.

```
figure; hold on; grid on;

% Start and end coordinates
X = [conductors(:,1), conductors(:,4)]';
Y = [conductors(:,2), conductors(:,5)]';
Z = [conductors(:,3), conductors(:,6)]';

phase = conductors(:,9);

for code = 1:3
    switch code
        case 1
            color_code='g';
        case 2
            color_code='r';
        case 3
            color_code='c';
    end
    idx = (phase == code);
    if any(idx)
        plot3(X(:, idx), Y(:, idx), Z(:, idx), ...
            'Color', color_code, ...
            'LineStyle', '-', 'LineWidth', 2, ...
            'Marker', 'o', 'MarkerSize', 2);
    end
end
hold off;
xlabel('X [m]'); ylabel('Y [m]'); zlabel('Z [m]');
```

MATLAB code 5.3: 3D visualization of conductors

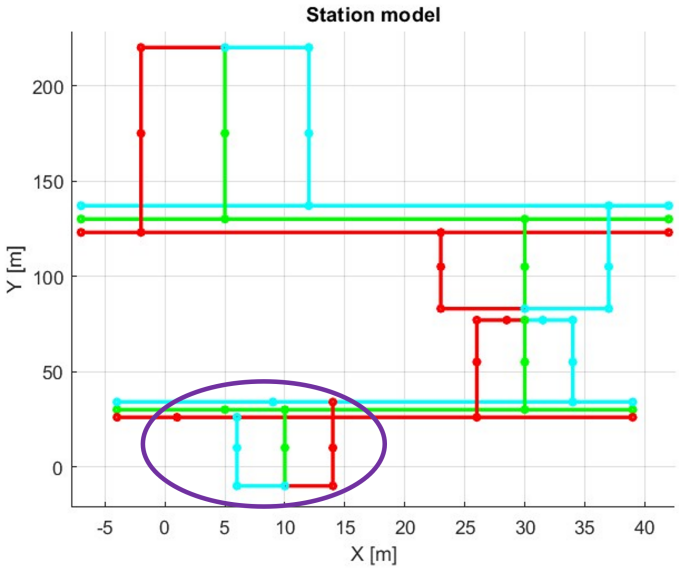

Figure 5.6: 3D conductor map for debugging.
Identified errors: (1) Incorrect phase sequence;
(2) Busbar supports misaligned with outgoing conductors

5.3.2 Current Map

This verifies the path and direction of current in each conductor of the substation. To graphically represent this information, a three-dimensional vector map is generated using the *quiver3* command. Conductors without current flow are identified as belonging to a fictitious "fourth phase" (and thus displayed with a specific color) to distinguish them from active conductors.

Current is defined as positive when flowing from P_1 to P_2. To determine current polarity, the phase angle (φ) must be evaluated within specific ranges according to the phase:

1. **Phase 1**: $-\frac{\pi}{2} < \varphi < \frac{\pi}{2}$,
2. **Phase 2**: $-\frac{\pi}{2} + \frac{2}{3}\pi < \varphi < \frac{\pi}{2} + \frac{2}{3}\pi$,
3. **Phase 3**: $-\frac{\pi}{2} - \frac{2}{3}\pi < \varphi < \frac{\pi}{2} - \frac{2}{3}\pi$.

The MATLAB code 5.4 performs the following operations:

1. Identifies the phase angle φ of current $\underline{\mathrm{I}}$
2. Normalizes the angle to the $0° - 360°$ range

3. Verifies the angle falls within $0° - 180°$ and inverts conductor coordinates if outside range

4. Plots the 3D current map

The graphical result is shown in Figure 5.7, where a case of incorrect polarity in one line is observed, as highlighted in the caption.

```
%Invert P1 and P2 for lines with I<0
n_lines=size(conductors,1);
for i = 1:n_lines
    current=conductors(i,7)+1j*conductors(i,8);
    magnitude=abs(i_complex);
    angle = rad2deg(angle(i_complex));
    %angle ranges between -180° and 180°
    phase=conductors(i,9)
switch phase     %Normalize phase angle range
    case 1
        angle=angle+90;
    case 2
        angle=mod(angle-120+90, 360);
    case 3
        angle=mod(angle+120+90, 360);
end         %now range is 0°-360°

    %1e-12 accounts for numerical error
    if magnitude<1e-12
    %if current is zero, define as "phase 4"
        conductors(i,9)=4;
    elseif angle > 180
    %invert P1 and P2
        conductors(i, [1 4]) = conductors(i, [4 1]);
        conductors(i, [2 5]) = conductors(i, [5 2]);
        conductors(i, [3 6]) = conductors(i, [6 3]);
    end
end
%Store in matrix P1, P2, phase
vectors=conductors(:,[1:6 7]);
vectors(:,4:6) = vectors(:,4:6) - vectors(:,1:3);


figure; hold on; grid on;
% Extract initial data and directions
X = vectors(:,1); Y = vectors(:,2); Z = vectors(:,3);
U = vectors(:,4); V = vectors(:,5); W = vectors(:,6);
phase = vectors(:,7);

for code = 1:4
    switch code
```

```
        case 1
            color_code='g';
        case 2
            color_code='r';
        case 3
            color_code='c';
        case 4
            color_code='m';
    end
    idx = phase == code;
    if any(idx)
        quiver3(X(idx), Y(idx), Z(idx), ...
            U(idx), V(idx), W(idx), 0,...
            'Color', color_code, ...
            'LineWidth', 1.5, 'MaxHeadSize', 0.5);
    end
end

hold off;
xlabel('X [m]'); ylabel('Y[m]'); zlabel('Z[m]');
```

MATLAB code 5.4: Current direction visualization

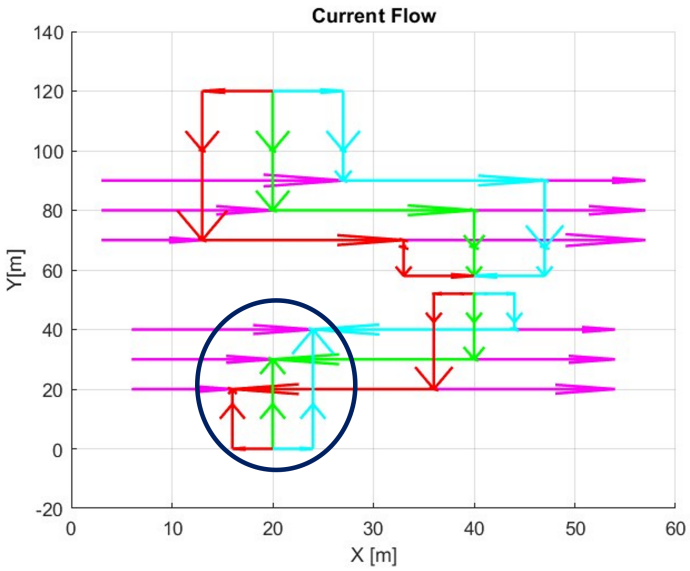

Figure 5.7: Current map

Detected error: outgoing line shows current direction opposite to expected

5.3.3 KCL

The previous maps validated the correct geometric arrangement of conductors and current flow direction. This section presents a quantitative analysis for system debugging, verifying compliance with Kirchhoff's Current Law (KCL).

KCL, or node law, states that the algebraic sum of currents entering a node must equal the sum of currents leaving:

$$\sum \underline{I}_{in} = \sum \underline{I}_{out} \tag{5.1}$$

This verification ensures physical continuity of conductors in the model and electrical correctness, excluding discontinuities or implementation errors. The implemented MATLAB code 5.5 performs:

1. Identifies nodes: for each conductor, endpoints P_1 and P_2 are compared with others to find connected nodes;
2. Balances currents: sums incoming and subtracts outgoing currents;
3. Verifies zero net current at each node, otherwise generates diagnostic plots.

```
%start and end point coordinates of each conductor
P1 = conductors(:,1:3);
P2 = conductors(:,4:6);
%Current expressed as phasor
currents = complex(conductors(:,7), conductors(:,8));
for i = 1:n_lines
    node1 = P1(i,:);
    node2 = P2(i,:);
    % Find rows corresponding to nodes
    out1 = all(P1 == node1, 2);
    in1 = all(P2 == node1, 2);
    out2 = all(P1 == node2, 2);
    in2 = all(P2 == node2, 2);
    %Calculate net current at node 1 and 2 (P1, P2)
    current1 = sum(currents(out1)) - sum(currents(in1));
    current2 = -sum(currents(out2)) + sum(currents(in2));
    %KCL is respected if net current is zero
    %1e-11 tolerance for numerical error
    if abs(current1) > 1e-11 || abs(current2) > 1e-11
    %KCL violated, save conductor index
        idx_error = [idx_error; i];
    end
end
if ~isempty(idx_error)
    ...%code for plotting conductors(idx_error,:)
end
```

MATLAB code 5.5: Node law verification

5.4 Substation Model

After entering the data, the code automatically processes the substation model, reconstructing current paths and conductor positions. Figures 5.8 5.9 5.10 5.11 show some examples of possible configurations that the code can model. Note the flexibility in modifying the number of busbars, transformers, lines and sections as needed. The figures demonstrate representations of single busbar, double busbar (with single or double breakers) and main-transfer busbars configuration.

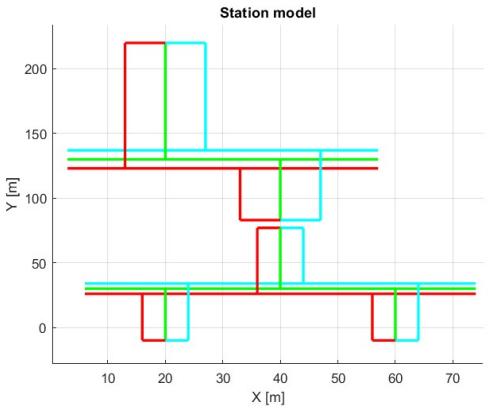

Figure 5.8: Single busbar substation model.

1 transformer, 1 incoming line, 2 outgoing lines

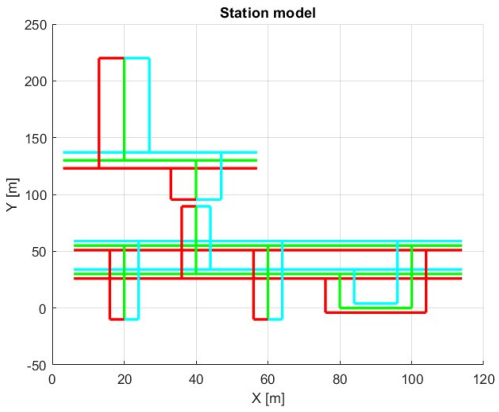

Figure 5.9: Main and transfer busbar substation model.

1 transformer, 1 incoming line, 2 outgoing lines, 1 bus coupler

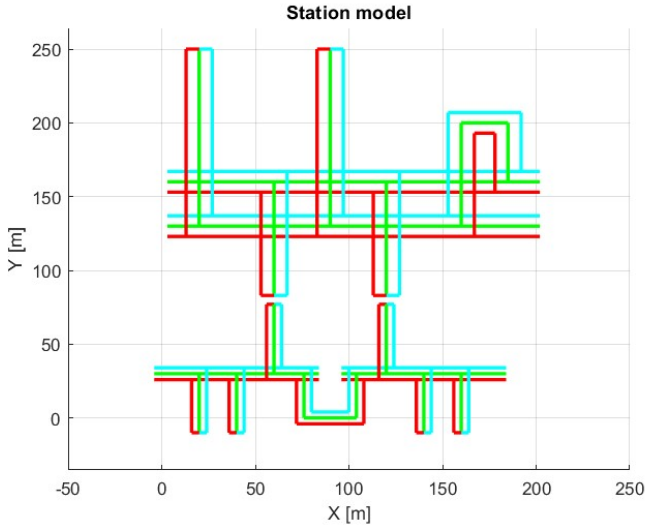

Figure 5.10: Double busbar (EHV) with single breaker and sectionalized single busbar (HV) model.

2 transformers, 2 incoming lines, 4 outgoing lines, 1 bus coupler (EHV), 1 bus sectionalizer (HV)

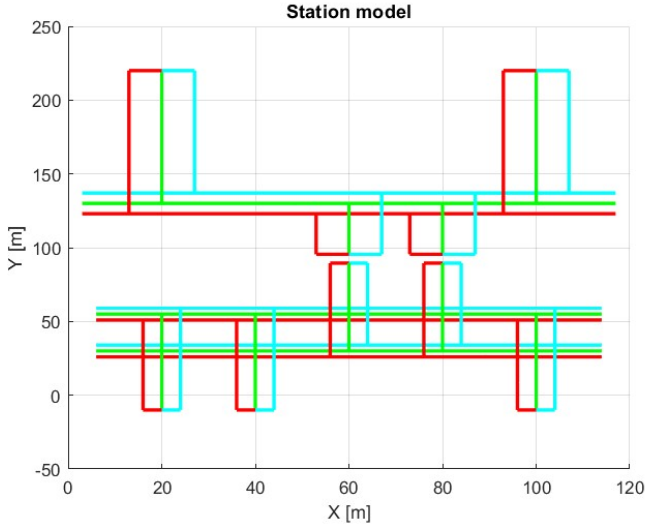

Figure 5.11: Single busbar (EHV) and double busbar (HV) with double breaker model

2 transformers, 2 incoming lines, 3 outgoing lines

5.5 Field Calculation Windows

After processing the substation model, the code generates two graphical interfaces (GUIs) dedicated to defining spatial regions for electric field (Figure 5.12) and magnetic field (Figure 5.13) evaluation. For the magnetic field, the complete and exact model is used since the far-field approximation (as demonstrated in the previous chapter) isn't applicable for all magnetic field values.

Users freely define the evaluation plane, with the only constraint being it must be parallel to one Cartesian plane (XY, YZ, or XZ). Region discretization is automatically optimized to minimize computation time while ensuring result accuracy. The user doesn't need to manually specify mesh granularity, making the process user-friendly and robust.

Field calculation results can be displayed using continuous color gradients or contour lines (isolines). Default levels comply with current regulations, but users can specify custom values separated by semicolons.

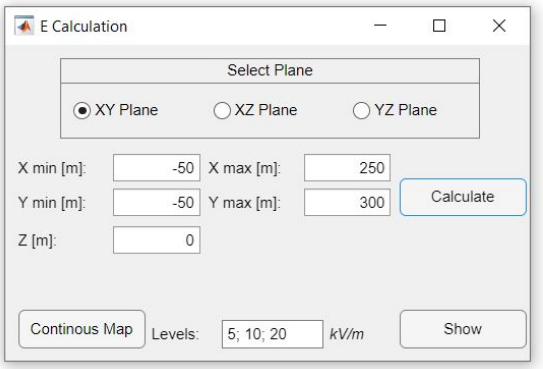

Figure 5.12: Electric field calculation window

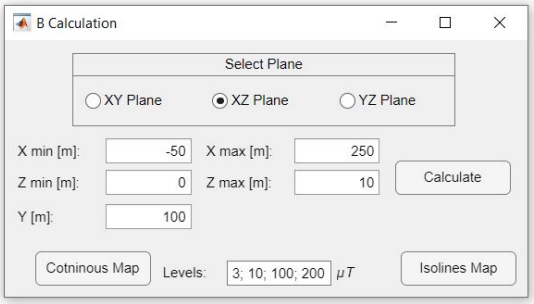

Figure 5.13: Magnetic field calculation window

Chapter 6

Case Study

This chapter presents a theoretical case study developed to validate the proposed MATLAB code and compare the models described in the previous chapters. The analysis focuses on an Air-Insulated Substation (AIS) operating at voltage levels of 380 kV / 150 kV. This specific substation was chosen for its representativeness in terms of both physical dimensions and operating currents, thus ensuring a meaningful test of the model under realistic conditions. The selection of an AIS substation reflects code optimization, as this typology requires accurate modeling of near-field effects around conductors, without the shielding typical of Gas-Insulated Substations (GIS).

The followed approach involves complete simulation with the integral model, followed by comparison with the simplified model, which is useful for quick safety distance estimates.

Although the case study focuses on a specific configuration, the code is designed to be parametric, allowing analysis of both existing substations (by inputting real geometries and operational data) and preliminary designs (by varying voltages, currents or component layouts).

The obtained results will be discussed in the next section, with graphs showing electromagnetic field trends and focusing on regulatory limits.

6.1 Typical design values for AIS

The adopted configuration is based on standard design values used by Terna SpA, according to their technical specifications [41]. This choice ensures consistency with industrial standards, facilitating comparison with real-world data and model integration in design phases.

6.1.1 Typical Conductor Cross-Sections

The main conductors (busbars and risers) are tubular-type, while bay conductors are typically made of bundled conductors, often multiple strands in parallel. Table 6.1 shows the characteristic diameters, with distinct values for each voltage level. For multi-strand bundled conductors, the equivalent diameter value is reported.

Table 6.1: Typical diameters of busbars and bays [41]

Element	**132–150 kV**	**220 kV**	**380 kV**
Busbar	100 mm	150 mm	220 mm
Line bay	36 mm	50 mm	60 mm
Transformer bay	50 mm	36 mm	60 mm
Busbar parallel section	50 mm	60 mm	60 mm

6.1.2 Typical Geometric Parameters

The substation geometry directly influences the electromagnetic field distribution. Table 6.2 summarizes key dimensions for three voltage levels, used in the MATLAB model to reconstruct the 3D structure.

Table 6.2: Typical geometric parameters by voltage level [41]

Parameter	**132-150 kV**	**220 kV**	**380 kV**
Phase-to-phase spacing	2,20 m	3,20 m	5,50 m
Busbar centerline spacing	10,40 m	14 m	22 m
Busbar height	7,50 m	9,30 m	11,80 m
Riser length	3 m	4 m	5,80 m
Line termination height	15 m	16 m	14 m
Bay width*	11 m	14 m	22 m
Busbar-to-line arrester distance	22 m	27,5 m	33,5 m

* The busbar parallel section occupies two bays.

6.1.3 Typical Current Values

The minimum rated thermal currents, as defined by Terna SpA standards, provide a useful parameter to understand the magnitude of currents in substations. Table 6.3 shows the distinct values for each component type and voltage level.

Table 6.3: Minimum rated thermal current by component type [41]

Component	**132-150 kV**	**220 kV**	**380 kV**
Busbar	2000 A	3150 A	4000 A
Circuit breaker bay	2000 A	2000 A	3150 A
Transformer bay	2000 A	1450 A	2000 A
Line bay	1250 A	2000 A	3150 A

6.2 Case Study Description: 380 kV / 150 kV AIS

The single-line diagram (Figure 6.1) shows a substation with the following characteristics:

- Double busbar with single circuit breaker configuration
- 2 incoming 380 kV lines (In = 600 A each)
- 6 outgoing 150 kV lines (In = 500 A each)
- 3 identical transformers (400 MVA, Vsc% = 13%, Yyn0)

Transient phenomena and harmonic effects are not considered, with analysis limited to sinusoidal conditions at power frequency. Protection devices (circuit breakers, disconnectors, surge arresters) were not modeled as they do not significantly affect the electric and magnetic fields, particularly in the far-field region.

This case study serves illustrative purposes and does not correspond to an existing substation, though it is based on real technical data. The adopted load conditions correspond to rated operating conditions.

The substation model computed by the code is shown in Figure 6.2 and Figure 6.3.

Field analysis was conducted at 1.5 m height, assumed as the reference level for human exposure assessment.

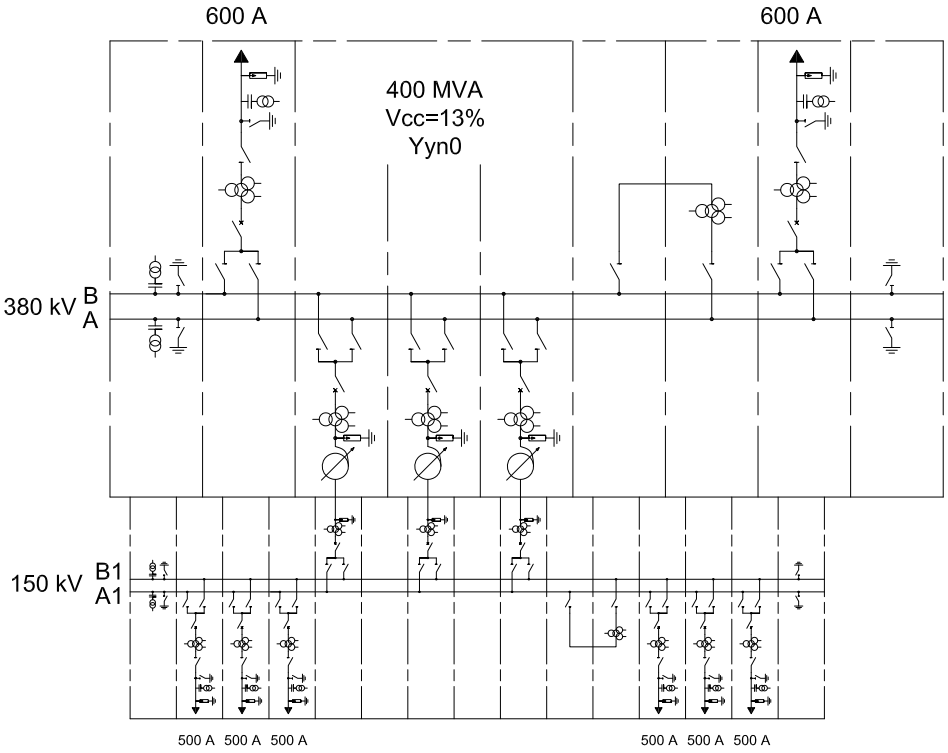

Figure 6.1: Single Line Diagram of the case study

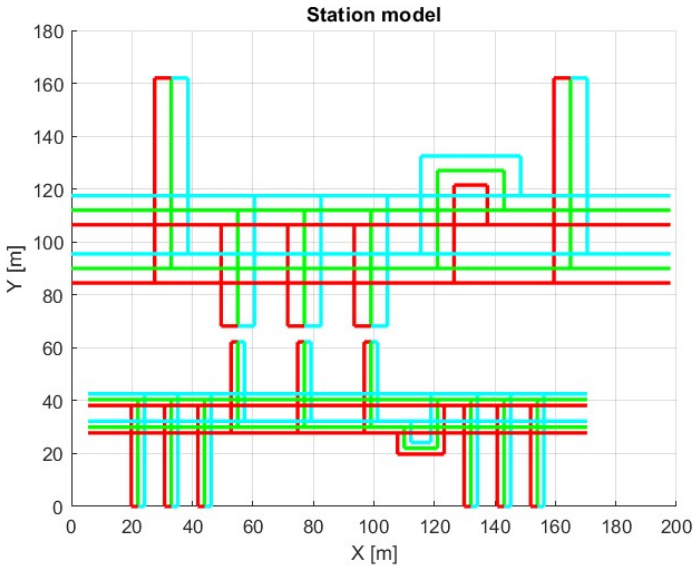

Figure 6.2: Top view of the case study substation model

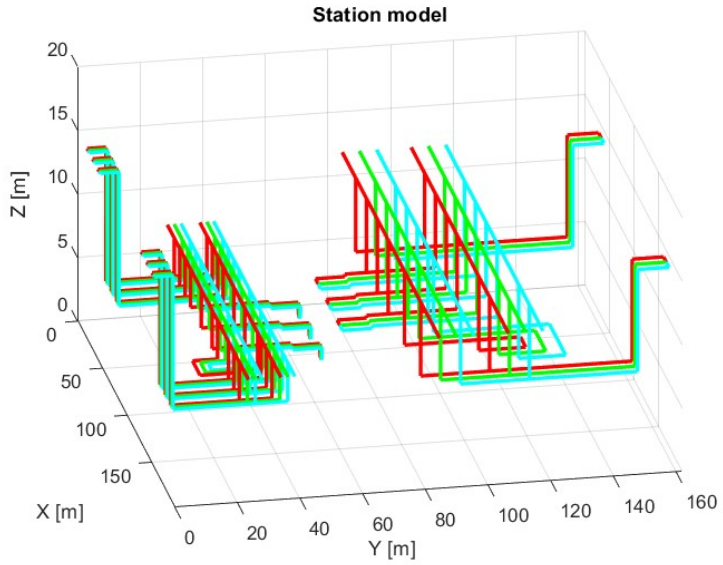

Figure 6.3: 3D model of the case study substation

6.3 Electric Field Analysis

The electric field analysis was performed under the most severe operating condition, with all busbars energized (primary and secondary double busbar) and load distributed between busbars, thus simulating full-load substation operation.

The evaluation was conducted on two types of planes:

- Horizontal plane at 1,5 m height, for quick assessment of human exposure at substation boundaries;
- Vertical planes, to identify critical zones near active components such as busbars and line bays.

As expected, the electric field generated by 380 kV conductors is significantly more intense than that produced by 150 kV conductors. This difference is clearly visible in Figure 6.4, which compares line bays at the two voltage levels. A similar behavior is observed when comparing the EHV busbar (380 kV, Figure 6.5) with the HV busbar (150 kV, Figure 6.6).

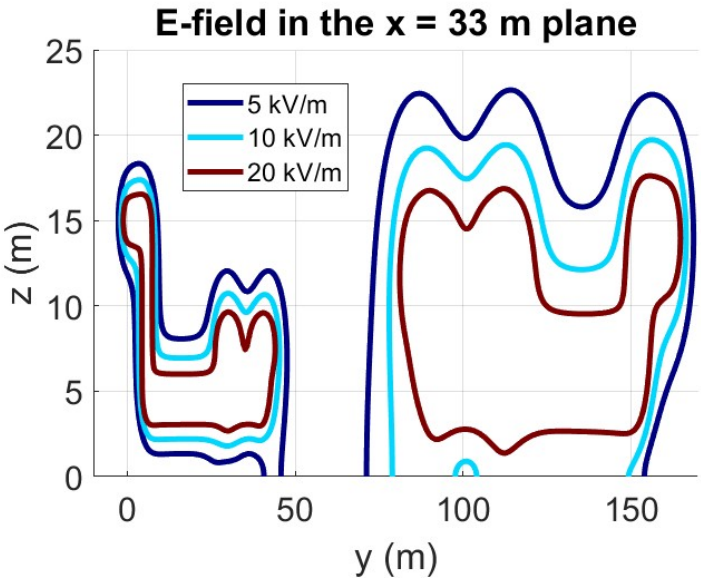

Figure 6.4: Electric field in the vicinity of line bays (HV and EHV)

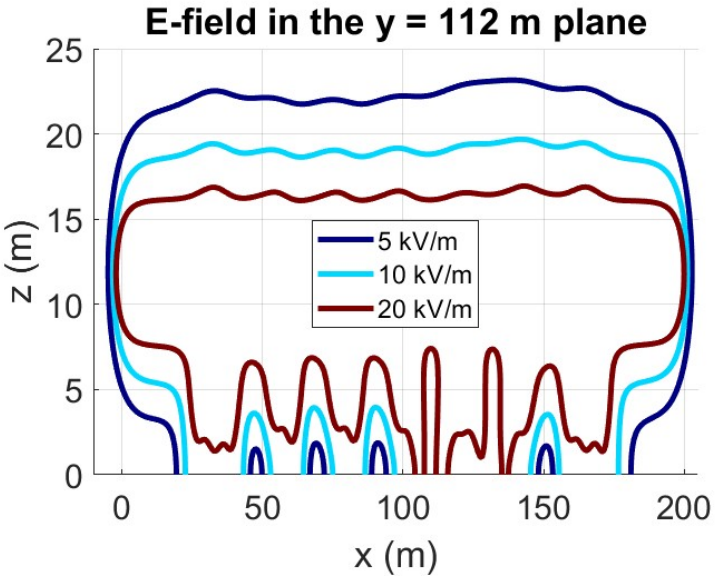

Figure 6.5: Electric field in the vicinity of the EHV busbar

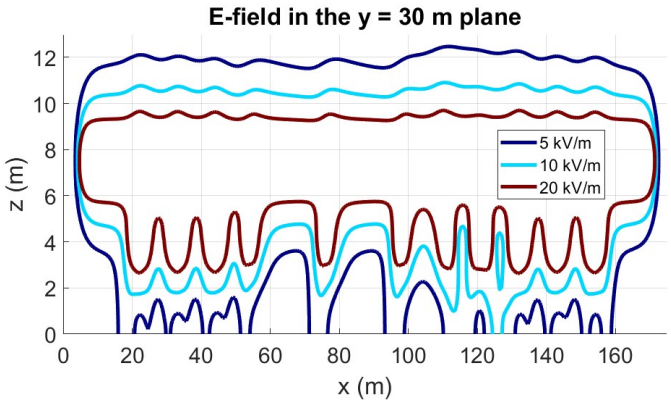

Figure 6.6: Electric field in the vicinity of the HV busbar

Regarding human exposure, Figure 6.7 shows the electric field at ground level (1,5 m height). The analysis - supported by Figure 6.8, which includes conductor projections - reveals that:

- There are no risks for the population outside the substation;
- Even for operational personnel, the electric field becomes negligible a few meters away from 150 kV conductors;
- For 380 kV conductors, greater distances are required to ensure acceptable exposure levels.

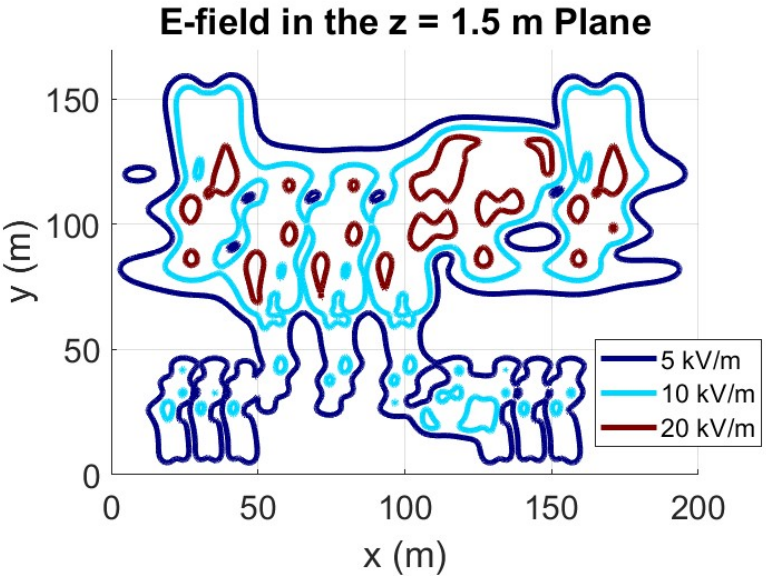

Figure 6.7: Electric field around the substation at $z = 1.5\,m$ height

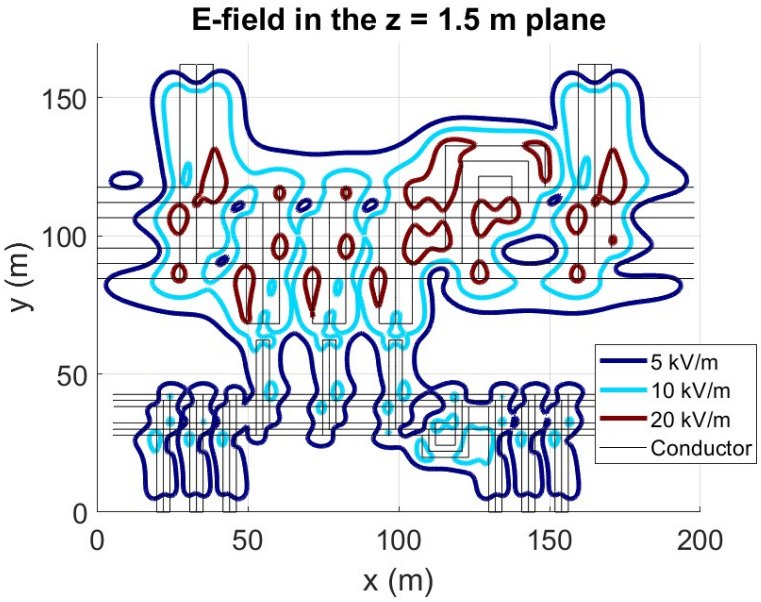

Figure 6.8: Electric field around the substation at $z = 1.5\,m$ height with substation conductor projections

6.4 Magnetic Field Analysis

This section analyzes the magnetic field generated by the substation in a meaningful configuration for public exposure assessment. In the considered scenario, only one busbar system is energized at both primary (380 kV) and secondary (150 kV) voltage levels. While it is possible for one busbar system to be de-energized due to faults or maintenance, the simultaneous de-energization of both voltage levels is extremely unlikely. Nevertheless, this configuration was chosen to obtain a conservative estimate of the magnetic field at the substation boundaries, thus ensuring protection for the general public who have no access to internal areas. To maximize the effect, the model was designed with all current flowing exclusively through the outermost busbars, i.e. the one closest to the substation perimeter.

Figure 6.9 shows only the current-carrying conductors, including their current flow direction.

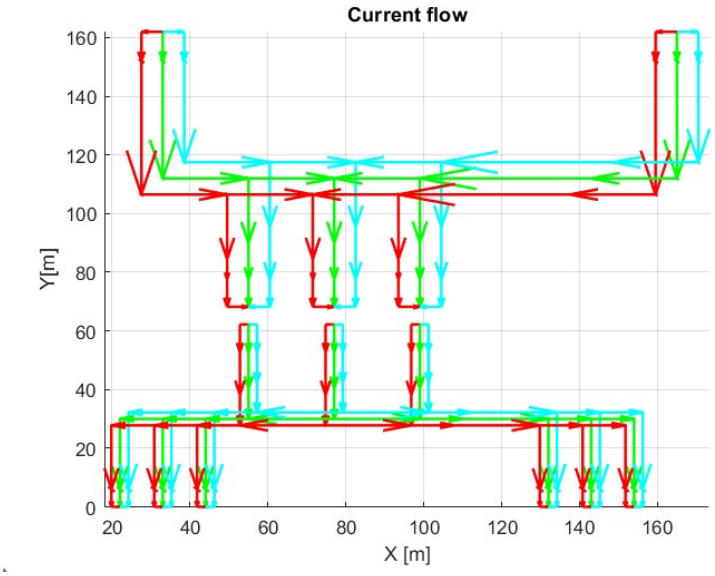

Figure 6.9: Current flow path in the B-field study configuration

The magnetic field assessment was conducted at different heights and on various planes to analyze field distribution near critical substation components and in publicly accessible areas. The analysis reveals that near line bays (Figure 6.10), the magnetic field shows higher values on the HV side, due to both higher current flow and greater phase spacing.

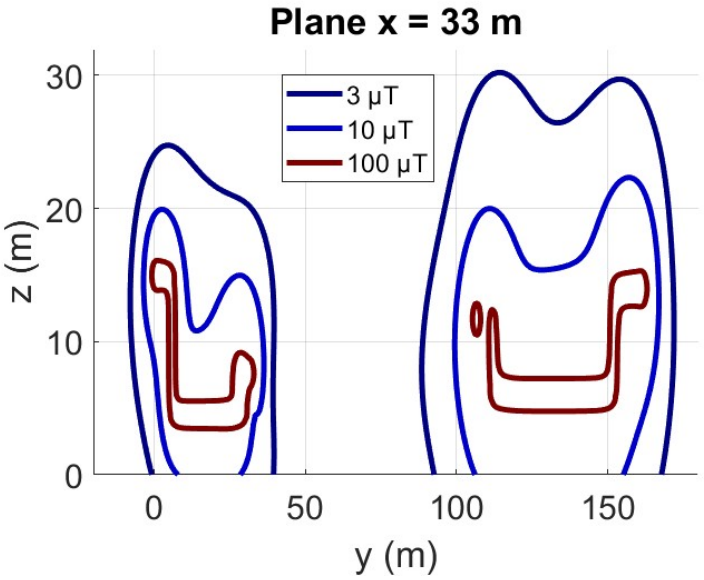

Figure 6.10: Magnetic field in the vicinity of line bays (HV and EHV)

For busbars, however, an opposite behavior is observed: the current in HV busbars is approximately 2.5 times higher than in EHV busbars, consistent with the transformation ratio ($380/150 \approx 2.5$). This is reflected in the field distribution, as shown in Figures 6.11 and 6.12.

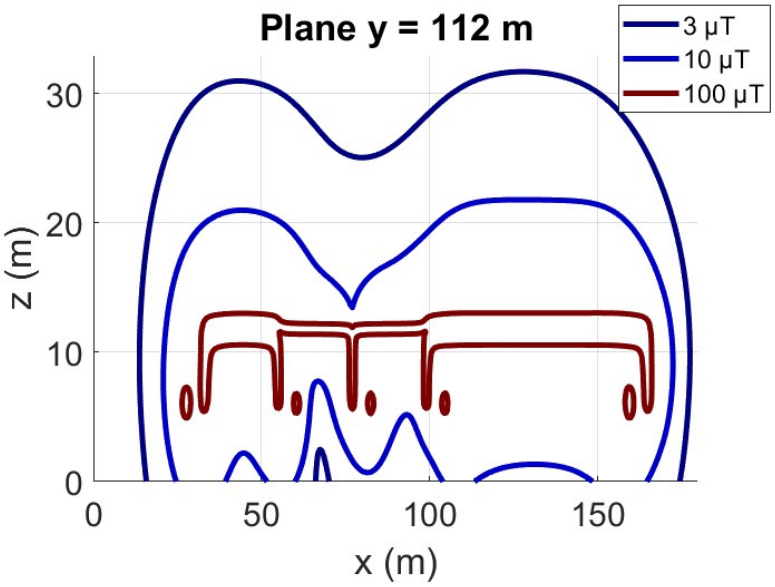

Figure 6.11: Magnetic field in the vicinity of the EHV busbar

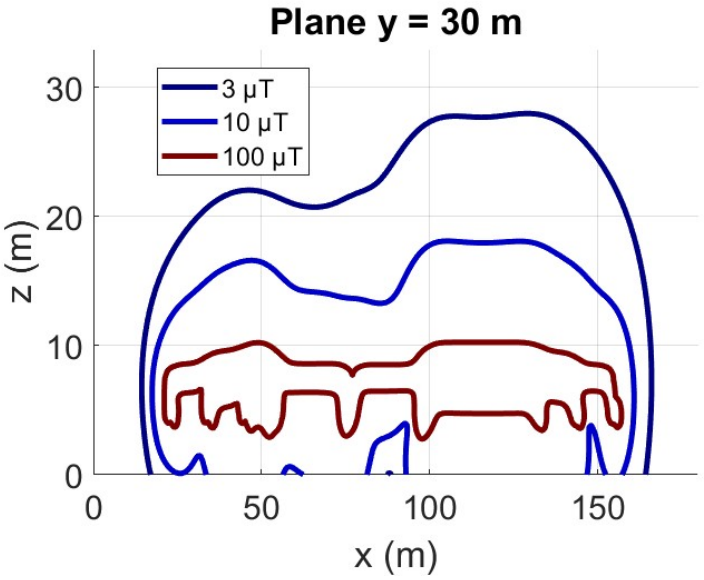

Figure 6.12: Magnetic field in the vicinity of the HV busbar

Finally, Figure 6.13 shows the magnetic field on a horizontal plane at 1.5 m height, corresponding to the average human height. Note that the 100 μT contour line is not present, as the elevated conductor height significantly reduces the magnetic field at ground level.

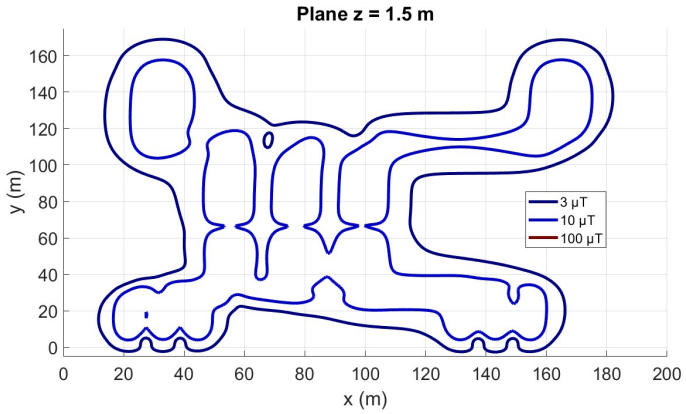

Figure 6.13: Magnetic field around the substation at $z = 1{,}5$ m height

6.5 Simplified B-Field Model

This section presents the calculation of the magnetic field using a simplified model based on the far-field approximation, with the objective of validating its effectiveness through systematic comparison with the exact model. Despite the significant simplifications introduced, the results demonstrate good agreement between the two approaches.

Figure 6.14 shows a direct comparison of the 3 μT contour lines computed on the $z = 1{,}5$ m plane using both models. The analysis reveals substantially coincident results, with limited errors that do not compromise the reliability of the estimate or the definition of the safety boundary. The most significant discrepancies are observed near conductor ends, where the simplified model's assumption (far-field approximation) introduces a conservative error that tends to overestimate the field in critical zones, thereby enhancing the safety assessment.

Figure 6.15 displays the 10 μT contour line on the same plane. In this case, the models agree well on the 150 kV side due to high currents and reduced phase spacing, while differences appear on the 380 kV side caused by greater phase spacing and lower currents, which position the 10 μT field in regions not fully compatible with the far-field approximation.

An additional analysis was conducted for the 100 μT contour (Figure 6.16), evaluated at a higher elevation ($z = 6$ m) where the field becomes significant. Here,

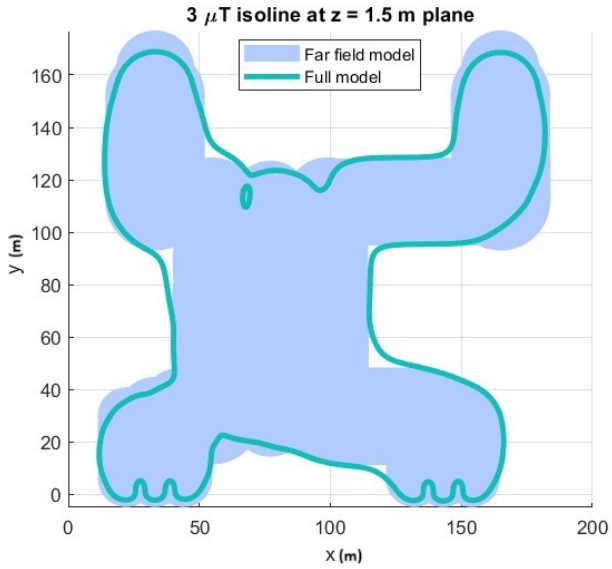

Figure 6.14: Model comparison at $B = 3\,\mu\mathrm{T}$ on the $z = 1.5\,\mathrm{m}$ plane

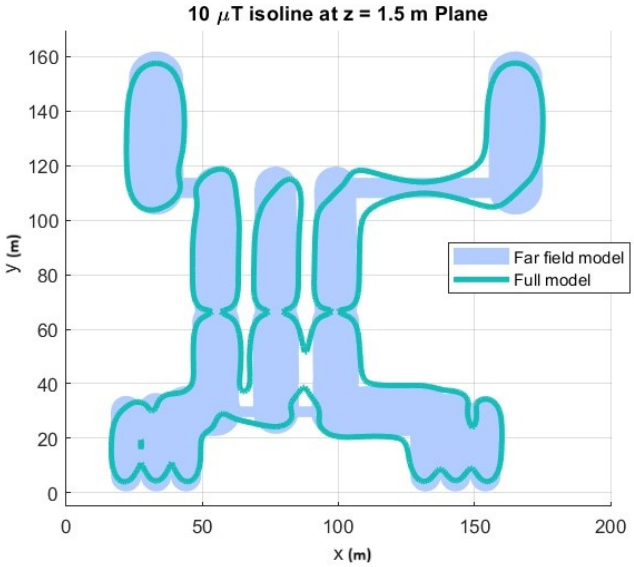

Figure 6.15: Model comparison at $B = 10\,\mu\mathrm{T}$ on the $z = 1.5\,\mathrm{m}$ plane

marked differences appear on the 380 kV side, with completely different contour shapes between models. Differences are also noticeable on the 150 kV side, though less pronounced.

In summary, the simplified model represents a valuable tool for designers, thanks

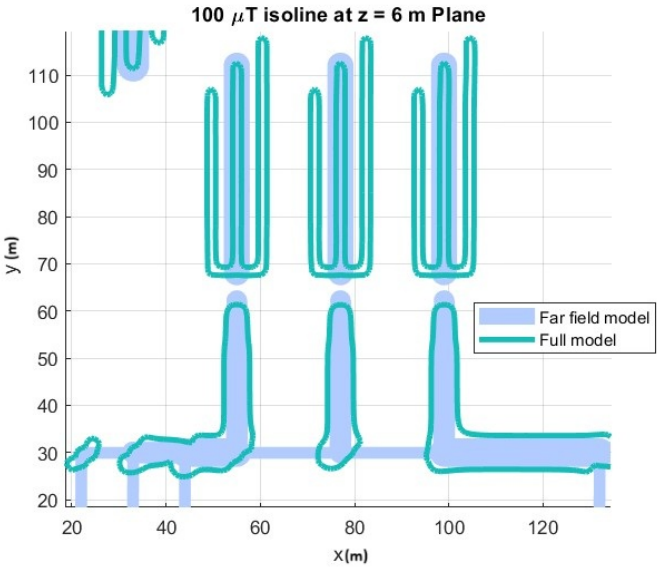

Figure 6.16: Model comparison at $B = 100\,\mu\mathrm{T}$ on the $z = 6\,\mathrm{m}$ plane

to its computational simplicity and immediate results. Despite the identified limitations, its use is recommended for preliminary magnetic field assessments.

Chapter 7

Conclusions

This thesis addresses the issue of electromagnetic pollution generated by High and Extra-High Voltage power substations, with a particular focus on evaluating human exposure to low-frequency electric and magnetic fields.

A numerical code was developed in a MATLAB environment, characterized by its flexibility and ease of use. This code reliably provides the spatial distribution of these fields, avoiding the complexity of more traditional methods like finite elements.

The approach is based on an integral formulation, which limits discretization to active conductors only, eliminating the need to discretize surrounding air or ground volumes. This significantly reduces the computational load without compromising accuracy in estimating safety distances, which are the distances within which field levels exceed current regulatory limits.

The code was applied to a theoretical case study involving a 380/150 kV AIS substation, allowing for the evaluation of electric and magnetic field levels and their spatial distribution, as well as compliance with regulatory limits.

The results demonstrated the effectiveness of the simplified model - which can be fastly applied with just "pen and paper" - for calculating the magnetic field, showing good reliability in estimating safety distances for low thresholds (3–10 μT). However, for higher thresholds (e.g. 100 μT), the estimation was less accurate due to the breakdown of far-field validity condition. The model proves to be an effective tool for the design of new substations, and its adoption is recommended.

The original contribution of this work lies in the development of the numerical code and a simple yet robust method capable of providing conservative estimates for preliminary design and regulatory verification, thereby addressing a gap in engineering practice. The proposed model enables a rapid and scientifically sound preliminary assessment, making it a valuable tool for designers, operators and technicians involved in the planning and verification of electrical infrastructure.

However, the work does present limitations, such as the inability to accurately

model GIS substations, which would require an extension of the model to account for interaction with metallic enclosures. Such a development could make the code even more versatile and complete, helping to support the design and regulation of electrical infrastructure in compliance with safety and sustainability criteria.

In conclusion, this thesis represents a step forward in electrical engineering design, integrating awareness of electromagnetic field exposure with simplicity, scientific rigor and practical applicability within a field of growing regulatory and technological relevance.

Ringraziamenti

Anche se la tesi è scritta in inglese, scrivo i ringraziamenti in italiano per rivolgermi diretamente a chi ha fatto parte di questo mio percorso.

Gli ultimi due anni sono stati intensi, traboccanti di vita in tutte le sue sfumature. Anni di gioie e di preoccupazioni, di sorprese e di paure, di passione e di fatica, di speranze che si accendono, di sogni che si evolvono e di tante nuove amicizie. Sono stati anni vissuti pienamente, che non sono passati inosservati e che, grazie a tutti voi, hanno plasmato la persona che sono oggi. Il Signore fa bene ogni cosa, e di questi due anni ne ha fatto un capolavoro.

Ringrazio il mio relatore, il Prof. Canova. Non è stato solo una guida accademica ma anche una presenza costante e un volto amico al Politecnico. Lo ringrazio per le sue parole di supporto e incoraggiamento, mai mancate lungo il percorso. Nonostante i suoi molteplici impegni, ha sempre trovato il tempo per seguirmi con attenzione, con una disponibilità, una competenza e una gentilezza mai scontate, sempre apprezzate. Mi ha dato spazio per esplorare e soprattutto ha creduto in me. È stato un piacere lavorarci insieme.

Ringrazio con tutto il cuore la mia famiglia. Ai miei genitori, per la loro presenza costante, il solido sostegno e la fiducia che mi hanno sempre dimostrato. Ai miei fratelli - Benedetto, Marco, Giovanni e Davide - per l'affetto sincero e il sostegno reciproco che non sono mai mancati. Ai nonni, gli zii, i cugini, Giovanna e Noemi, che sono stati i miei più grandi tifosi; sempre vicini e certi del buon esito di questo percorso.

Ringrazio i compagni di studi conosciuti a Torino, con i quali ho costruito relazioni autentiche e condiviso molte ore, sia tra i banchi che al di fuori dell'università. Un grazie particolare va a Ignazio, compagno di studi da dieci anni, nonché il primo volto amico ritrovato a Torino.

Ringrazio gli amici di lunga data, quelli che ho ritrovato a Torino e quelli che sono rimasti tali nonostante la distanza. È sempre una festa rivedervi, ritrovarsi in una chiacchierata sincera e continuare a condividere affetto, fiducia e risate come un tempo.

Un grazie va anche agli amici incontrati a Bruxelles: Paola, Francesca, Pietro, Celeste, Pablo, Isabelle... In particolare a Maria, compagna di tanti lunghi viaggi in autobus. Sui sedili del 60, persi per le strade di una città straniera, cercavamo insieme di orientarci nella vita. Grazie alla famiglia Bordoni, una famiglia vivace e allegra che con semplicità e naturalezza mi hanno fatto sentire a casa. E grazie a Sara, mia coinquilina, compagna di pasti improvvisati e di lunghe chiacchierate in quello stanzino che chiamavamo cucina. In ogni tuo bussare al tuo rientro a casa e in ogni conversazione, c'era quel calore umano che ha riscaldato un freddo e strano gennaio.

Ringrazio le comunità che ho incontrato lungo il mio percorso: quella in Sicilia, quella di Torino, in cui ho trovato un rifugio sicuro, quella di Breslavia e quella di Bruxelles, dove sono stato accolto con entusiasmo e profondità. In ognuna di queste realtà ho trovato volti, storie, legami che sono stati come un balsamo dolce, capace di dare senso e forza anche nei momenti più difficili.

Il mio augurio per ciò che verrà è che io possa custodire e mettere a frutto tutto ciò che questi anni mi hanno dato. Che la conoscenza acquisita, gli incontri vissuti, le lezioni imparate – di ingegneria e di vita – possano essere al servizio del bene e del prossimo. Per la gloria di Dio e per un mondo migliore.

Bibliography

[1] Presidenza del Consiglio dei Ministri. *Fissazione dei limiti di esposizione, dei valori di attenzione e degli obiettivi di qualita' per la protezione della popolazione dalle esposizioni ai campi elettrici e magnetici alla frequenza di rete (50 Hz) generati dagli elettrodotti*. Tech. rep. Online; accessed 12-May-2025. Governo Italiano, 2003. URL: https://www.gazzettaufficiale.it/eli/id/2003/08/29/03A09749/sg (cit. on pp. 1, 18, 44, 46).

[2] International Commission on Non-Ionizing Radiation Protection (ICNIRP). «ICNIRP Guidelines for Limiting Exposure to Time-Varying Electric and Magnetic Fields (1 Hz to 100 kHz)». In: *Health Phys.* 99.6 (2010), pp. 818–836. DOI: 10.1097/HP.0b013e3181f06c86 (cit. on pp. 1, 4, 8, 14).

[3] Working Group C4.204. *Mitigation techniques of power frequency magnetic fields originated from electric power systems*. Tech. rep. International Council on Large Electric Systems (CIGRE), 2009. DOI: 11696/31675 (cit. on p. 1).

[4] D. Andreuccetti and N. Zoppetti. «Magnetic fields dispersed by high-voltage power lines: An Advanced evaluation method based on 3-D models of electrical lines and the territory». In: *Radiat. Prot. Dosimetry* 111.4 (2004), pp. 343–347. DOI: 20.500.14243/22466 (cit. on p. 1).

[5] G. Filippopoulos and D. Tsanakas. «Analytical calculation of the magnetic field produced by electric power lines». In: *IEEE Trans. Power Delivery* 20.2 (2005), pp. 1474–1482. DOI: 10.1109/TPWRD.2004.839184 (cit. on p. 1).

[6] R. K. Z. Sahbudin, S. A. Fauzi, S. Hitam, and M. Mokhtar. «Investigation of electrical potential and electromagnetic field for overhead high voltage power lines in Malaysia». In: *J. Appl. Sci.* 10.22 (2010), pp. 2862–2868. DOI: 10.3923/jas.2010.2862.2868 (cit. on p. 1).

[7] Z. Du, J. Ruan, Z. Gan, X. Ruan, R. Rong, L. Nie, L. Zhou, and C. Liao. «Three-dimensional numerical simulation of power frequency electromagnetic field inside and outside substation». In: *Power Syst. Technol.* 36.4 (2012), pp. 229–235 (cit. on p. 1).

[8] M. Grbić, A. Canova, and L. Giaccone. «Levels of Magnetic Field in an Apartment near 110/35 kV Substation and Proposal of Mitigation Techniques». In: *Proc. 10th Mediterranean Conf. on Power Generation, Transmission, Distribution and Energy Conversion*. Paper No. 030. Belgrade, Serbia, Nov. 2016. DOI: 10.1049/cp.2016.1025 (cit. on p. 1).

[9] M. Grbić, A. Pavlović, D. Hrvić, and B. Vulević. «Levels of Electric and Magnetic Fields inside 110/x kV Substations». In: *CIRED – Open Access Proc. J.* 2017.1 (2017), pp. 747–751. DOI: 10.1049/oap-cired.2017.1292 (cit. on p. 1).

[10] K. Gryz, J. Karpowicz, and K. Zajdler. «Evaluation of Electromagnetic Exposure during Workers' Activities near High-Voltage Electricity Grids». In: *Electromagnetic Ergonomics: from Electrification to a Wireless Society*. CRC Press, 2023, pp. 55–73. DOI: 10.1201/9781003020486-4 (cit. on p. 1).

[11] P. E. Munhoz-Rojas, C. S. Segura-Salas, A. A. Costa, R. Martins, and J. Hoffmann-Neto. «Fields and Current Densities Induced in the Human Body by Low-Frequency Electromagnetic Fields». In: *Proc. 2018 IEEE Int. Symp. on Electromagnetic Compatibility and 2018 IEEE Asia-Pacific Symp. on Electromagnetic Compatibility (EMC/APEMC)*. Suntec City, Singapore, 2018, pp. 1267–1273. DOI: 10.1109/ISEMC.2018.8393992 (cit. on p. 4).

[12] International Commission on Non-Ionizing Radiation Protection (ICNIRP). «ICNIRP Guidelines for Limiting Exposure to Electromagnetic Fields (100 kHz to 300 GHz)». In: *Health Phys.* 118.5 (2020), pp. 483–524. DOI: 10.1097/HP.0000000000001210 (cit. on p. 4).

[13] Office of Engineering and Technology (OET), FCC. *Questions and Answers about Biological Effects and Potential Hazards of Radiofrequency Electromagnetic Fields*. OET Bulletin 56, Fourth Edition. [Online; accessed 29-May-2025]. Aug. 1999. URL: https://transition.fcc.gov/Bureaus/Engineering_Technology/Documents/bulletins/oet56/oet56e4.pdf (cit. on pp. 4, 6).

[14] J. Patrick Reilly. *Applied Bioelectricity: From Electrical Stimulation to Electropathology*. New York: Springer, 1998. DOI: 10.1007/978-1-4612-1664-3 (cit. on pp. 7, 9).

[15] K. R. Foster. «Mechanisms of Interaction of Extremely Low Frequency Electric Fields and Biological Systems». In: *Radiation Protection Dosimetry* 106.4 (2003), pp. 301–310. DOI: 10.1093/oxfordjournals.rpd.a006364 (cit. on pp. 8–11).

[16] International Commission on Non-Ionizing Radiation Protection (ICNIRP). «Guidelines for Limiting Exposure to Time-varying Electric, Magnetic, and Electromagnetic Fields (up to 300 GHz)». In: *Health Physics* 74.4 (1998). Online; accessed 04-July-2025, pp. 494–522. URL: https://www.icnirp.org/cms/upload/publications/ICNIRPemfgdl.pdf (cit. on p. 10).

[17] Nancy Wertheimer and Ed Leeper. «Electrical wiring configurations and childhood cancer». In: *American Journal of Epidemiology* 109.3 (1979), pp. 273–284. DOI: 10.1093/oxfordjournals.aje.a112681 (cit. on p. 11).

[18] Anders Ahlbom et al. «A pooled analysis of magnetic fields and childhood leukaemia». In: *British Journal of Cancer* 83.5 (2000), pp. 692–698. DOI: 10.1054/bjoc.2000.1376 (cit. on p. 12).

[19] Leeka Kheifets et al. «Pooled analysis of recent studies on magnetic fields and childhood leukaemia». In: *British Journal of Cancer* 103.7 (2010), pp. 1128–1135. DOI: 10.1038/sj.bjc.6605838 (cit. on p. 12).

[20] GyeongAe Seomun, Juneyoung Lee, and Jinkyung Park. «Exposure to extremely low-frequency magnetic fields and childhood cancer: A systematic review and meta-analysis». In: *PLOS ONE* 16.5 (2021), e0251628. DOI: 10.1371/journal.pone.0251628 (cit. on p. 12).

[21] Aryana T. Amoon, John Swanson, Corrado Magnani, Christoffer Johansen, and Leeka Kheifets. «Pooled analysis of recent studies of magnetic fields and childhood leukemia». In: *Environmental Research* 204 (2022), p. 111993. DOI: 10.1016/j.envres.2021.111993 (cit. on p. 12).

[22] F. Parazzini, L. Tozzi, R. Mezzopane, C. La Vecchia, L. Fedele, and L. Bocciolone. «Video display terminal use during pregnancy and reproductive outcome–a meta-analysis». In: *Journal of Occupational Medicine* 35.5 (1993), pp. 476–480. DOI: 10.1136/jech.47.4.265 (cit. on p. 13).

[23] G. M. Shaw and L. A. Croen. «Human adverse reproductive outcomes and electromagnetic field exposures: review of epidemiologic studies». In: *Environmental Health Perspectives* 101.Suppl 4 (1993), pp. 107–119. DOI: 10.1289/ehp.93101s4107 (cit. on p. 13).

[24] Michael B. Bracken, Kathleen Belanger, Karen Hellenbrand, Larry Dlugosz, Theodore R. Holford, Jean-Ellen McSharry, Karen Addesso, and Brian Leaderer. «Exposure to Electromagnetic Fields During Pregnancy with Emphasis on Electrically Heated Beds: Association with Birthweight and Intrauterine Growth Retardation». In: *Epidemiology* 6.3 (1995), pp. 263–270. DOI: 10.1097/00001648-199505000-00013 (cit. on p. 13).

[25] T. S. Tenforde. «Interaction of ELF magnetic fields with living systems». In: *Handbook of Biological Effects of Electromagnetic Fields*. Ed. by C. Polk and E. Postow. 2nd. CRC Press, 1996, pp. 185–230. DOI: 10.1201/9781351071017 (cit. on p. 13).

[26] D. A. Savitz, H. Checkoway, and D. P. Loomis. «Magnetic field exposure and neurodegenerative disease mortality among electric utility workers». In: *Epidemiology* 9.4 (1998), pp. 398–404. DOI: 10.1097/00001648-199807000-00009 (cit. on p. 13).

[27] Christoffer Johansen and Jørgen H. Olsen. «Risk of cancer among Danish utility workers–a nationwide cohort study». In: *American Journal of Epidemiology* 147.6 (1998), pp. 548–555. DOI: 10.1093/oxfordjournals.aje.a009486 (cit. on p. 13).

[28] Nils Håkansson, Per Gustavsson, Lennart Hallin, Birgitta Feychting, and Anders Floderus. «Neurodegenerative Diseases in Welders and Other Workers Exposed to High Levels of Magnetic Fields». In: *Epidemiology* 14.4 (2003), pp. 420–426. DOI: 10.1097/01.EDE.0000078446.76859.c9 (cit. on p. 13).

[29] Council of the European Union. *Council Recommendation of 12 July 1999 on the limitation of exposure of the general public to electromagnetic fields (0 Hz to 300 GHz)*. Official Journal of the European Communities. Online; accessed 04-June-2025. 1999. URL: https://eur-lex.europa.eu/eli/reco/1999/519/oj (cit. on p. 15).

[30] European Parliament and Council of the European Union. *Directive 2013/35/EU of the European Parliament and of the Council of 26 June 2013 on the minimum health and safety requirements regarding the exposure of workers to the risks arising from physical agents (electromagnetic fields)*. Official Journal of the European Union. Online; accessed 15-May-2025. 2013. URL: https://eur-lex.europa.eu/eli/dir/2013/35/oj (cit. on p. 15).

[31] Repubblica Italiana. *Legge 22 febbraio 2001, n. 36: Legge quadro sulla protezione dalle esposizioni a campi elettrici, magnetici ed elettromagnetici*. Gazzetta Ufficiale della Repubblica Italiana. Online; accessed 12-May-2025. 2001. URL: https://www.gazzettaufficiale.it/eli/id/2001/03/07/001G0084/sg (cit. on p. 17).

[32] Repubblica Italiana. *Decreto Legislativo 9 aprile 2008, n. 81 – Attuazione dell'art. 1 della legge 3 agosto 2007, n. 123, in materia di tutela della salute e della sicurezza nei luoghi di lavoro*. Tech. rep. Online; accessed 12-May-2025. Governo Italiano, 2008. URL: https://www.normattiva.it/uri-res/N2Ls?urn:nir:stato:decreto.legislativo:2008;81!vig= (cit. on p. 18).

[33] Commissione Elettrotecnica Internazionale. *CEI EN 60038: Tensioni nominali di riferimento*. Norma europea armonizzata. 2012 (cit. on p. 20).

[34] Phil Bolin. «Gas-Insulated Substations». In: *Electric Power Substations Engineering*. Ed. by John D. McDonald. 3rd ed. Boca Raton, FL: CRC Press, 2012, pp. 2.1–2.19. DOI: 10.1201/b12061-2 (cit. on pp. 28, 29, 31).

[35] European Parliament and Council of the European Union. *REGULATION (EU) 2024/573 OF THE EUROPEAN PARLIAMENT AND OF THE COUNCIL of 7 February 2024 on fluorinated greenhouse gases, amending Directive (EU) 2019/1937 and repealing Regulation (EU) No 517/2014*. https://eur-lex.europa.eu/legal-content/EN/TXT/?uri=CELEX:32024R0573. [Online; accessed 29-May-2025]. 2024 (cit. on p. 28).

[36] E.R.A. Baig. *Gas Insulated Substation (GIS) vs Conventional Outdoor Substation (AIS)*. Tech. rep. Accessed May 2025. Barqaab Engineering Services, 2004. URL: https://www.barqaab.com/mainwebsite/Technical%20Papers/Gas%20Insulated%20VS%20Conventional.pdf (cit. on p. 30).

[37] T. Sakakibara, K. Terasaka, T. Yoshida, and I. Miwa. «Distribution of Induced Grounding Current in Large-Capacity GIS Using Multipoint Grounding System». In: *IEEE Transactions on Power Delivery* PWRD-1.4 (Oct. 1986), pp. 120–127. DOI: 10.1109/TPWRD.1986.4308038 (cit. on pp. 32, 33).

[38] T. Sauramaki, T. Keikko, S. Kuusiluoma, and L. Korpinen. «Exposure to electric and magnetic fields at 110 kV gas insulated substation (GIS)». In: *IEEE/PES Transmission and Distribution Conference and Exhibition*. Vol. 2. 2002, pp. 1226–1229. DOI: 10.1109/TDC.2002.1177653 (cit. on p. 34).

[39] Aldo Canova and Giambattista Gruosso. «3D source simulation method for static fields in inhomogeneous media». In: *International Journal for Numerical Methods in Engineering* 70.9 (2007), pp. 1096–1111. DOI: https://doi.org/10.1002/nme.1923 (cit. on pp. 36, 37).

[40] A. Canova, F. Freschi, M. Repetto, and M. Tartaglia. «Description of power lines by equivalent source system». In: *COMPEL - The International Journal for Computation and Mathematics in Electrical and Electronic Engineering* 24.3 (2005), pp. 893–905. DOI: 10.1108/03321640510598210 (cit. on p. 39).

[41] Terna S.p.A. *Technical Specification: Requirements and reference characteristics of substations and power lines of the National Transmission Grid*. Accessed May 2025, in italian. May 2015. URL: https://download.terna.it/terna/0000/0105/20.pdf (cit. on pp. 47, 65–67).

[42] Davide Bavastro, Aldo Canova, Luca Giaccone, and Michele Manca. «Integral and analytical models for evaluating the distance of compliance». In: *International Journal of Numerical Modelling: Electronic Networks, Devices and Fields* 27.3 (2013), pp. 590–599. DOI: 10.1002/jnm.1941 (cit. on p. 47).

[43] A. Canova, L. Giaccone, M. Manca, R. Turri, and P. Casagrande. «Simplified power transformer models for environmental magnetic impact analysis». In: *2nd International Conference on EMF-ELF*. Paris, France, Mar. 2011. DOI: 11577/176331 (cit. on p. 47).

[44] Davide Bavastro, Aldo Canova, Luca Giaccone, and Michele Manca. «Simulazione e sperimentazione di schermature magnetiche per infrastrutture elettriche». In: *Campi elettromagnetici e innovazione tecnologica in ambito difesa, industria e ricerca: atti del convegno*. Pisa: Pisa University Press, 2013, pp. 121–124. DOI: 10.1400/220943 (cit. on p. 47).